EUROPEAN ORGANIZATION FOR NUCLEAR RESEARCH

CERN-EP/83-94
July 14th 1983

MEASUREMENT OF PRODUCTION AND PROPERTIES OF JETS AT THE CERN $\bar{p}p$ COLLIDER

The UA2 Collaboration

P. Bagnaia[b], M. Banner[f], R. Battiston*,£, Ph. Bloch[f], F. Bonaudi[b], K. Borer[a], M. Borghini[b], J.-C. Chollet[d], A.G. Clark[b], C. Conta[e], P. Darriulat[b], L. Di Lella[b], J. Dines-Hansen[c], P-A. Dorsaz[b], L. Fayard[d], M. Fraternali[e], D. Froidevaux[b], G. Fumagalli[e], J-M. Gaillard[d], O. Gildemeister[b], V.G. Goggi[e], B. Hahn[a], H. Hänni[a], J.R. Hansen[b], P. Hansen[b,c], T. Himel[b], V. Hungerbühler[b], P. Jenni[b], O. Kofoed-Hansen[c], E. Lançon[f], M. Livan[b,e], S. Loucatos[f], B. Madsen[c], P. Mani[a], B. Mansoulié[f], G.C. Mantovani*, L. Mapelli$^{\psi}$[b], B. Merkel[d], R. Møllerud[c], C. Onions[b], G. Parrour[b,d], F. Pastore H. Plothow-Besch[b,d], M. Polverel[f], J-P. Repellin[d], A. Rimoldi[e], A. Rothenberg[b], A. Roussarie[f], G. Sauvage[d], J. Schacher[a], J.L. Siegrist[b], H.M. Steiner†[b], G. Stimpfl[b], F. Stocker[a], J. Teiger[f], V. Vercesi[e], A. Weidberg[b], H. Zaccone[f] and W. Zeller[a].

a) Laboratorium für Hochenergiephysik, Universität Bern, Sidlerstrasse 5, Bern, Switzerland.

b) CERN, 1211 Geneva 23, Switzerland.

c) Niels Bohr Institute, Blegdamsvej 17, Copenhagen, Denmark.

d) Laboratoire de l'Accélérateur Linéaire, Université de Paris-Sud, Orsay, France.

e) Dipartimento di Fisica Nucleare e Teorica, Università di Pavia and INFN, Sezione di Pavia, Via Bassi 6, Pavia, Italy.

f) Centre d'Etudes Nucléaires de Saclay, France.

* Gruppo INFN del Dipartimento di Fisica dell'Università di Perugia (Italy).

† On leave from Dept. of Physics, University of California, Berkeley.

£ Also at Scuola Normale Superiore, Pisa, Italy.

ψ On leave from INFN, Pavia, Italy.

Submitted to Zeitschrift für Physik C

ABSTRACT

The production and properties of high transverse momentum hadron jets have been measured in the UA2 experiment at the CERN $\bar{p}p$ Collider ($\sqrt{s}$ = 540 GeV) using a highly segmented total absorption calorimeter. The characteristics of a sample of two-jet events with invariant mass up to 200 GeV/c^2 are discussed, including measurements of their fragmentation properties, angular and rapidity distributions, and the properties of the additional energy clusters accompanying the two-jet system. Cross sections for inclusive jet production in the jet transverse momentum range between 30 and 100 GeV/c and for the two-jet invariant mass distrition in the mass range from 60 to 200 GeV/c^2 are reported.

1 - INTRODUCTION

The suggestion that the hard scattering of hadron constituents should result in the production of two jets having the same momenta as the scattered partons [1] has motivated intense experimental efforts [2]. The increasing importance of jet production in hadron collisions at high energy was realized when large transverse momentum (p_T) processes [3] in early ISR experiments were interpreted in terms of jet production and fragmentation [4]. However, unambiguous identification of jets in hadronic collisions has been reported only recently by the UA2 [5] and the UA1 [6] experiments at the CERN $\bar{p}p$ Collider observing the emergence of two-jet dominance in very large transverse energy $\bar{p}p$ collisions, and by two ISR experiments [7]. A comparison of hadron jets produced in hadron-hadron, lepton-hadron and electron-positron collisions is given in Ref. [8].

We report here results from the UA2 experiment. The very successful operation of the CERN $\bar{p}p$ Collider [9] at $\sqrt{s}$ = 540 GeV during the 1982 period has enabled us to accumulate a data sample about 200 times larger than in the previous period of data collection in 1981. The present data not only confirm the dominance of two-jet configurations in events having large transverse energy measured in the central region as found previously in the UA2 experiment [5], but also allow a first study of their most outstanding properties.

The article is organized as follows. After a short introduction to the UA2 apparatus in Sect. 2, we describe the data collection and reduction procedure in Sect. 3. The dominant two-jet structure of the events is demonstrated in Sect. 4. In Sect. 5, we discuss measurements related to jet fragmentation : charged particle multiplicities, transverse momentum distribution of jet fragments, and radial and longitudinal energy flow distributions. Production properties of two-jet systems are presented in Sect. 6 where we study their transverse and longitudinal momenta and their angular distribution. Section 7 is devoted to an analysis of the underlying event structure in two-jet events and to a study of additional correlated jets. Finally, inclusive jet and two-jet production cross sections are given in Sect. 8, and conclusions are summarized in Sect. 9.

2 - DETECTOR AND DATA TAKING

2.1 - Apparatus.

The UA2 detector assembly is shown schematically in Fig. 1.

The vertex detector, a set of cylindrical wire chambers densely packed around the beam in the collision region, provides measurements of the position of the event vertex and of the directions of the charged particles produced in the collision. It is made of four proportional chambers with helicoidal cathode strips and of two drift chambers of 24 azimuthal cells each, with six drift wires per cell. A fifth similar proportional chamber, preceded by 1.5 radiation lengths of tungsten, is used for shower localization in front of the electromagnetic calorimeter.

The vertex detector is surrounded by a highly segmented electromagnetic and hadronic calorimeter (the central calorimeter) that covers the pseudo-rapidity interval $-1 < \eta < 1$ (polar angles $40^{\circ} < \theta < 140^{\circ}$) and an azimuthal ($\phi$) range of 300°. The present data were taken in a configuration where the remaining azimuthal interval of $\pm 30^{\circ}$ around the horizontal plane, Fig. 1b, is covered by a single arm spectrometer (wedge detector) which is used to measure charged and neutral particle production [10] and jet fragmentation.

The forward and backward regions ($20^{\circ} < \theta < 37.5^{\circ}$ and $142.5^{\circ} < \theta < 160^{\circ}$, respectively), are each instrumented by twelve toroidal magnet sectors followed by drift chambers, multitube proportional chambers and electromagnetic calorimeters.

The central calorimeter is segmented into 200 cells, each covering 15° in ϕ and 10° in θ and built in a tower structure pointing to the centre of the interaction region. The cells are segmented longitudinally into a 17 radiation length thick electromagnetic compartment (lead-scintillator) followed by two hadronic compartments (iron-scintillator) of two absorption lengths each. The light from each compartment is collected by two BBQ-doped light guide plates on opposite sides of the cell.

All calorimeters, including the forward modules, have been calibrated in a 10 GeV/c beam from the CERN PS using incident electrons and muons. The calibration has since been tracked with a Xe light flasher system and by measuring the average energy flow into each module for

unbiased $\bar{p}p$ collisions. In addition, the response of the electromagnetic compartments is checked regularly by accurately positioning a Co^{60} source in front of each cell and measuring the direct current from each photomultiplier. The systematic uncertainty in the energy calibration for the data discussed here is less than ±2% for the electromagnetic calorimeter and less than ±4% for the hadronic one.

The response of the calorimeter to electrons, single hadrons and multi-hadrons (produced in a target located in front of the calorimeter) has been measured at the CERN PS and SPS machines using beams from 1 to 70 GeV/c. In particular we have studied the longitudinal and transverse shower development and the effect of particles impinging near the cell boundaries.

The energy resolution for electrons is measured to be $\sigma_E/E = 0.14/\sqrt{E}$ (E in GeV). In the case of hadrons, σ_E/E varies from 32% at 1 GeV to 11% at 70 GeV, approximately proportional to $E^{-\frac{1}{4}}$. The resolution for multi-hadron systems of more than 20 GeV is similar to that of single hadrons.

Details of the construction and performance of the calorimeter are reported elsewhere [11].

The wedge detector is a single-arm large-angle magnetic spectrometer in the horizontal plane covering 28° in ϕ and 68° in θ (± 0.7 units in rapidity) symmetrically around $\theta = 90^\circ$ with respect to the colliding beams. The magnet occupies the space of four central calorimeter modules that have been removed for that purpose. The calorimeter is used as a return yoke. The field integral is about 1 Tm. The charged particle trajectories are measured before the magnet with the vertex detector, and after in a set of 12 large drift chamber planes. The momentum resolution is $\sigma_p/p \simeq 0.01\ p$ (p in GeV/c). These chambers are followed by a scintillator-iron-scintillator sandwich and by a 14 radiation lengths thick lead-glass wall.

2.2 - Data taking.

The data discussed in this paper were recorded using a trigger sensitive to events with large transverse energy (ΣE_T) in the central calorimeter. The gains of the photomultipliers were adjusted so that their signals were proportional to transverse energy. The signals were linearly

added and their sum was required to exceed a given threshold set at 25 GeV for an integrated luminosity ($\int \mathcal{L} dt$) of 1.8 nb^{-1} and at 35 GeV for $\int \mathcal{L} dt = 13.3\ nb^{-1}$.

In order to suppress background from sources other than $\bar{p}p$ collisions we required a coincidence with two signals obtained from scintillator arrays covering an angular range $0.47^{\circ} < \theta < 2.84^{\circ}$ on both sides of the collision region [12].

A sample of "minimum bias" data was recorded simultaneously by using only the coincidence of the signals from the two scintillator arrays. The rate of such coincidences provided also a measurement of the luminosity [12].

Furthermore, the electronics were enabled between $\bar{p}p$ crossings and the cosmic ray background was found to be negligible.

3 - DATA REDUCTION

3.1 - Event selection criteria.

The events collected with the large transverse energy trigger (ΣE_T) include a small background contamination from sources other than $\bar{p}p$ collisions. This contamination varies from 5 to 15% depending on the running conditions of the $\bar{p}p$ Collider. Beam halo particles can either satisfy the triggering condition directly or appear as an accidental overlap with a "minimum bias" $\bar{p}p$ interaction.

The background events exhibit a characteristic pattern in the detector different from that of large ΣE_T $\bar{p}p$ events. They are rejected from the data sample by two selection criteria :

i) if they are associated with an early signal in the small angle scintillator arrays ;

ii) if they have an abnormally large total transverse energy fraction in the hadronic compartments (more than 60% in the second one or more than 95% in both together).

These requirements reduce the background contamination in the data sample to < 5% independent of ΣE_T. The loss of good events introduced by the cuts is negligible. This fact has been established by studies using minimum bias events for the time-of-flight requirement and test beam data for the energy deposition criteria.

3.2 - Transverse energy distribution.

The response of the electromagnetic calorimeter compartment to energy deposited by photons (or electrons) differs from that of hadrons by typically 20%, depending on energy. We have adopted a constant set of weighting factors (1.18, 1.00, 1.06) for the three compartment energies (electromagnetic, first and second hadronic) that optimizes the resolution and linearity of the calorimeter response to high energy hadrons as described in detail in Ref. [11].

The total hadronic energy in a cell of the calorimeter is measured as the weighted sum of the energies in the three compartments where each compartment entering the sum must exceed 150 MeV, well above pedestal fluctuations.

The distribution of events as a function of the total transverse energy ΣE_T (summed over all cells) in the pseudo-rapidity interval $-1 < \eta < 1$ and in the azimuthal acceptance $30^o < \phi < 330^o$ is presented in Fig. 2. The transverse energies have been calculated with respect to the centre of the detector. The event vertex has been reconstructed for a sample of the events used for the cross section measurements (Sect. 8). Its distribution along the $\bar{p}p$ beam axis is well centered in the detector and has a rms spread of ±10 cm. No acceptance correction has been applied to the data shown in Fig. 2. We estimate that the uncertainty in the energy scale of ΣE_T due to systematic effects (150 MeV minimum compartment energy requirement, calibration errors, neglecting event vertex position) is less than ±10%.

The ΣE_T distribution of Fig. 2 shows a clear departure from exponential when ΣE_T exceeds $\sim$ 60 GeV, an effect not seen in lower energy experiments [7,13].

4 - TWO-JET DOMINANCE

4.1 - Energy clustering.

In order to investigate the pattern of energy distribution in the events we adopt, as in our previous analysis [5], a straight-forward clustering algorithm taking advantage of the fine granularity of

the calorimeter segmentation. We join into a cluster all cells which share a common side and have a cell energy $E_{cell} > E_{cell}^{min}$. E_{cell}^{min} is normally chosen to be 400 MeV, though the results obtained are relatively insensitive to its exact value. Clusters having two or more local maxima separated by a valley deeper than 5 GeV are then split. In each event we rank the clusters in order of decreasing transverse energies and denote them by $E_T^1 > E_T^2 > E_T^3 \ldots$. The clusters contain typically 3 cells for E_T = 2 GeV and 10 cells for E_T = 40 GeV.

4.2 - Two-jet Structure.

The mean values of the fractions $h_1 = E_T^1/\Sigma E_T$ and $h_2 = (E_T^1 + E_T^2)/\Sigma E_T$ are shown in Fig. 3a as a function of ΣE_T. Their behaviour illustrates the emergence of a dominant two-jet structure at large values of ΣE_T. An event containing only two jets of equal transverse energies would have $h_1 = 0.5$ and $h_2 = 1$. The dependence on ΣE_T of the ratios $r_{21} = E_T^2/E_T^1$ and $r_{32} = E_T^3/E_T^2$, (Fig. 3b) shows the same effect. As ΣE_T increases, r_{21} approaches about 0.8 whereas r_{32} decreases significantly. A large fraction of the total transverse energy of large ΣE_T events is shared on average by two clusters only.

The azimuthal separation $\Delta\phi_{12}$ between the two clusters having the largest transverse energies per event (E_T^1 and E_T^2) is shown in Fig. 4 for events with $\Sigma E_T > 60$ GeV and E_T^1, $E_T^2 > 20$ GeV. The distribution of $\Delta\phi_{12}$ is observed to peak near 180° showing that the two clusters are approximately back-to-back in the transverse plane.

Direct evidence for two-jet dominance is also obtained from an inspection of the transverse energy distribution in the ϕ-θ plane. As an example Fig. 5 shows the configuration of the event with the largest value of ΣE_T, 213 GeV. The transverse energy is concentrated within two small regions (Fig. 5a) which are separated in azimuth by $\Delta\phi_{12} = 180^\circ$ and towards which several collimated tracks are observed to point (Fig. 5b).

5 - JET FRAGMENTATION

The event configuration displayed in Fig. 5b, where a high particle density is associated with each cluster of large transverse energy, is a general feature of the present data. This suggests the presence of hadron jets resulting from the fragmentation of scattered partons. In the present Section we investigate some properties of the observed jets and compare them with those of quark jets produced in e^+e^- collisions.

5.1 - Charged particle multiplicity in jets.

The vertex detector measures the charged particle multiplicity in jets. Its angular coverage is much larger than that of the central calorimeter : it extends down to $\theta = 20^\circ$ and over the full azimuthal range. As a result the charged particle multiplicity measurement is almost free of acceptance corrections.

The main uncertainties in this measurement arise from two sources :

i) the efficiency of the vertex detector and of the associated pattern recognition algorithm has to be evaluated, especially in regions of high particle density,

ii) a procedure has to be defined to decide which of the observed tracks are to be associated with the jet and which are not.

In order to address these problems, our analysis is restricted to the transverse plane, where the track reconstruction efficiency is highest, and where particles not associated with the jet are expected to contribute a uniform azimuthal distribution.

Events are considered in which two clusters, each having a transverse energy in excess of 15 GeV and $\Delta\phi_{12} > 150^\circ$ (Sect. 4.2), are observed in the central calorimeter. Distributions of the azimuthal separation $\Delta\phi$ between each track observed in the vertex detector and the centroid of the highest transverse energy cluster are shown in Fig. 6 for two intervals of M_{jj}, the invariant mass associated with the two highest energy clusters. Clear peaks are seen at $\Delta\phi \simeq 0$ and $\Delta\phi \simeq \pi$, as expected for two-jet events. The distribution is more peaked for the larger M_{jj} slice, showing that higher energy jets are more collimated. The distribution in $\Delta\phi$ is not symmetric about $\Delta\phi = \pi/2$. This is partly explained by the fact

that the two jets are not exactly back-to-back in the transverse plane. Secondly a broad high multiplicity jet will tend to have less energy found in a leading calorimeter cluster than a more collimated lower multiplicity jet. Therefore in selecting the highest transverse energy cluster there is a bias favouring the selection of the narrower, lower multiplicity jet.

The transverse track finding efficiency of the vertex detector was measured in the azimuthal range covered by the wedge spectrometer by comparing the tracks reconstructed in each of these detectors for field off data. The efficiency was found to be 96 ± 2% and the fraction of spurious tracks was 7 ± 1%. The loss of tracks from the finite two-track resolution ($\sim$ 5 mm) was estimated from the distribution of the azimuthal separation between pairs of neighbour tracks, and evaluated to be $\sim$ 20%. The data were also corrected for γ conversions and π^0 Dalitz decays.

As a check on this procedure the mean charged particle multiplicity was measured for minimum bias events and compared with results obtained by the UA5 collaboration [14] in the same pseudo-rapidity range ($|\eta| < 2$). The result, 15.3 ± 0.7, is in reasonable agreement with the UA5 measurement, 13.45 ± 0.15, considering that the present data are not corrected for strange particle decays.

As illustrated in Fig. 6 the track density $\rho(\Delta\phi) = \frac{dN}{d(\Delta\phi)}$ is approximately constant over a large $\Delta\phi$ range around $\Delta\phi = \pi/2$, where it takes a value ρ_0. On the average ρ_0 is measured to be ~ 2 times as large as in minimum bias events. Particles not associated with the jets are assumed to contribute a uniform distribution to $\rho(\Delta\phi)$, $\lambda\ \rho_0$. This assumption was checked by measuring the track density in the polar angle regions $20^\circ < \theta < 37.5^\circ$ and $142.5^\circ < \theta < 160^\circ$ using the forward-backward drift chambers, for events containing a jet near $\theta = 90^\circ$. The distribution of $\Delta\phi$, the azimuthal separation between the forward-backward tracks and the highest transverse energy cluster is flat. A priori, λ may take any value between 0 and 1. The contribution of jet fragments near $\Delta\phi = \pi/2$ to the ρ-distribution, $\frac{dN}{d(\Delta\phi)} = (1-\lambda)\rho_0$, is directly related to their density with respect to the rapidity y^* measured along the common axis of the two jets in their c.m.s. near $y^* = 0$. If λ, or equivalently the y^* density, were known, we would be able to measure the average jet charged particle multiplicity as

$$n_{ch} = \tfrac{1}{2}\int_0^{\pi} \{\ \rho(\Delta\phi) - \lambda\rho_0\ \}\ d(\Delta\phi) \qquad (1)$$

To avoid the bias caused by the asymmetric $\Delta\phi$ distribution discussed above we define the jet multiplicity as the average multiplicity of the two jets. Lacking knowledge of λ, we use two different approaches to the problem :

i) we evaluate a lower bound of n_{ch} by setting $\lambda = 1$ in Eq (1). The values obtained are displayed in Fig. 7a and include only the leading jet fragments. They are compared with e^+e^- data [15] which we have modified according to Eq (1) using the measured value of $\frac{dN}{dy^*}$ in e^+e^- collisions to evaluate ρ_0 and using the fact that $\lambda = 0$ in e^+e^- two-jet final states.

ii) we evaluate n_{ch} from Eq (1) for two different estimates of λ, one for quarks and one for gluons, using a reasonable fragmentation model [16]. The results are shown in Fig. 7b and compared with e^+e^- [17] and pp [18] data. From a range of fragmentation models we observe that there is a 10% variation in the value of n_{ch}. The difference between the two evaluations reflects the higher y^* density for gluon than for quark fragments near $y^* = 0$. The e^+e^- measurements are also shown for comparison. The errors shown in Fig. 7 are purely statistical. We estimate the systematic error in the correction procedure (two track resolution, spurious tracks, track efficiency) to be $\sim$ 10%. The uncertainty caused by the asymmetric $\Delta\phi$ distribution is < 10%, for an overall systematic uncertainty of ±15%.

Both approaches indicate a larger charged particle multiplicity in the present sample of jets than in jets observed in e^+e^- collisions at lower energies. Even if λ were equal to one, which would imply that jet fragments do not populate the central $y^* \simeq 0$ region at all, the charged particle multiplicity of the jets observed in our data would be as large as that of e^+e^- jets. These results are consistent with expectations based on QCD calculations which predict that at relatively low $x_T = 2E_T/\sqrt{s}$ gluon jets having higher multiplicities than quark jets [16,19] tend to dominate [20] in $\bar{p}p$ collisions.

5.2 - Energy flow.

The difficulty of identifying large angle jet fragments without ambiguity is of lesser importance when evaluating the energy flow with respect

to the jet axis : large angle fragments carry only a small fraction of the jet energy. To illustrate this point two-jet events are selected with each jet having a transverse energy in excess of 15 GeV, and such that at least one of them (called A) is well contained within the central calorimeter acceptance. The distribution of the azimuthal transverse energy density, $\frac{dE_T}{d\Delta\phi}$, integrated over a rapidity interval of ±0.7 units around cluster A is shown in Fig. 8 for several intervals of the transverse energy E_T of cluster A. (Here $\Delta\phi$ is measured with respect to cluster A centroid and extends over the hemisphere opposite to the wedge detector in order to ensure full acceptance). No corrections have been made for acceptance or for granularity (shower and cell sizes), which are not expected to introduce a significant dependence on E_T. The peak near $\Delta\phi = 0$ increases with E_T. The density around $\Delta\phi = \frac{\pi}{2}$ is about 2.5 times larger than in minimum bias events and amounts to $\sim$ 7 GeV per $\Delta y \cdot \Delta\phi = 2\pi$.

The strong concentration of energy in the neighbourhood of the jet axis justifies the cluster algorithm described earlier as a way to obtain a good approximation of the jet energy. Nevertheless the $\frac{dE_T}{d\Delta\phi}$ distribution exhibits a significant tail and part of the jet energy may occasionally be excluded from the leading cluster. In order to study the shape of this tail in more detail a sample of events was selected in which a large transverse energy cluster is observed in the central calorimeter in such a position that any particle produced at angles $\psi < 40^\circ$ with respect to the cluster centroid falls within the calorimeter acceptance. The distribution of the normalised energy density, $\frac{1}{E}\frac{dE}{d\psi^2}$, is shown in Fig. 9 for two intervals of the cluster energy E. The data show a slight shrinking of the peak near $\psi = 0$ with increasing cluster energy. We stress however that the effect is partly obscured by the finite calorimeter cell size and shower radius which preclude a reliable measurement of the jet aperture in the angular range $\psi < 10^\circ$.

To quantitatively describe the tails of the transverse energy density distributions, the observed angular aperture of the leading clusters are compared with the prediction of a Monte Carlo calculation using a simple description of the fragmentation mechanism and simulating the details of the calorimeter response. We define a cluster aperture

$$\Omega = (\Sigma E_i \ \omega_i^2 / \Sigma E_i)^{\frac{1}{2}} \qquad (2)$$

where the sum extends over the cells in the cluster, each cell containing

A sample of 60 events is retained, with the jets having an average E_T of 25 GeV. In order to remove tracks not associated to the two-jet system, only those charged tracks are retained which carry at least 10% of the longitudinal jet momentum ($z > 0.1$).

The experimental distributions are compared to two Monte Carlo simulations. The first one uses the simple fragmentation model of the previous Section, eq. (3), and the second one is a QCD inspired model [21] for $\bar{p}p$ interactions with the parameters of the fragmentation functions [22] set to the standard values which best fit the e^+e^- data at PETRA. Figure 11 shows that the observed transverse momentum distribution and the longitudinal fragmentation distribution of the charged particles are well reproduced. The observed q_T^2 distribution, the square of the transverse momenta of the fragments with respect to the jet axis, is shown in Fig. 12. The limited acceptance of the wedge detector precludes a good measurement of the tails of the q_T^2 distribution. The low q_T^2 region ($q_T^2 < 0.5$ GeV^2) can be reproduced by the fragmentation model of eq. (3) with a slope parameter λ corresponding to an average value of q_T of 420 ± 40 MeV.

The fragmentation model of eq. (3) is not adequate to describe the tails observed in Fig. 12 for $q_T^2 > 0.5$ GeV^2. The experimental data are consistent with the prediction of the model [21] which includes final state gluon radiation.

5.4 - Longitudinal energy deposition.

Further evidence for jets is obtained from the measurement of the longitudinal distribution of energy deposition within the calorimeter. On the average jets are expected to deposit their energy earlier in the calorimeter than single charged hadrons of the same energy. This results from the presence of π^0's among the jet fragments and from the fact that each charged fragment carries only a fraction of the total jet energy and therefore generates a shorter hadronic shower within the calorimeter. Defining $E_{e.m.}$ and E_{H1} respectively as the cluster energies contained in the electromagnetic and first hadronic compartments of the calorimeter, the quantity

$$X = E_{e.m.}/(E_{e.m.} + E_{H1}) \qquad (4)$$

an energy E_i and separated by an angle ω_i from the cluster centroid. The distribution of Ω for two-jet events having $E_T^1 + E_T^2 > 40$ GeV is shown in Fig. 10. Simple fragmentation models assuming a distribution

$$\frac{dN}{dq_T^2} \propto e^{-\lambda q_T^2} \qquad (3)$$

for the transverse momenta q_T of the fragments with respect to the jet axis do not reproduce the tail observed at $\Omega \gtrsim 0.3$. This tail implies more energy at large q_T than provided by (3). One way to account for it is to allow for a first split in two jets with a $\frac{dN}{dq_T} \propto q_T^{-1}$ law, and to let both of these jets subsequently fragment according to (3). Such a behaviour is expected from gluon bremsstrahlung which will receive some support from the subsequent analysis of three-jet events (see Section 7).

5.3 - Transverse momentum of fragments.

The wedge detector, despite its relatively small angular coverage, provides a measurement of the fragments emitted at a small angle ($\lesssim 30^\circ$) to the jet axis. This measurement requires selecting events with a jet reasonably well contained within the wedge detector acceptance.

Since there was no total energy trigger in the wedge, events are selected using a special trigger requiring a transverse energy deposition in an azimuthal interval of the central calorimeter opposite to the wedge ($120^\circ < \phi < 240^\circ$). The transverse energy in the wedge is computed by adding the transverse momenta of the charged particle tracks reconstructed in the spectrometer and the transverse energy of neutral particles found from the lead glass clusters not associated to charged particles. The jet axis is defined by the vector sum of the momenta of all the charged and neutral particles detected in the wedge.

In order to select two-jet events with one of the jets well contained in the wedge the following selection criteria are imposed :

- there is at least one cluster with $E_T > 18$ GeV in the central calorimeter in the restricted azimuthal interval $150^\circ < \phi < 210^\circ$,
- the total transverse energy measured in the wedge exceeds 15 GeV,
- and the reconstructed jet axis is well contained inside the aperture of the wedge ($|\phi| < 10^\circ$ and pseudo-rapidity $|\eta| < 0.45$).

The components P_ξ^{jj} and P_η^{jj} of $\vec{P}_T^{jj}$, measured along two axes, ξ and η, chosen as the bisectors of the two transverse jet momenta (Fig. 14a), are studied separately because they are associated with different sources of systematic uncertainties. Their distributions, for the selected sample of 454 two-jet events, are shown in Fig. 14. Also shown are the Monte Carlo results using $< P_T^{jj} > = 5$ GeV/c.

The Monte Carlo simulation allows an evaluation of the ability of our detector to measure P_ξ^{jj} and P_η^{jj} by comparing generated and observed distributions. The average broadening is indicated by horizontal arrows on Fig. 14 and calls for two comments :

i) large observed values of P_T^{jj} are mostly of instrumental origin, which precludes a reliable measurement of the tail of the P_T^{jj} distribution,

ii) the measurement of P_η^{jj}, related to the azimuthal angle between the jet axes, is more accurate than that of P_ξ^{jj} which is directly affected by energy measurement errors and acceptance losses.

The data are found consistent with the hypotheses that $\vec{P}_T^{jj}$ has a uniform azimuthal distribution and that $dN/d(P_T^{jj})^2$ has a Gaussian dependence upon P_T^{jj}. Under such hypotheses, the mean value of P_T^{jj} is found to be $< P_T^{jj} > = 5 \pm 2$ GeV/c, where the uncertainty is mostly systematic and of instrumental origin. Splitting the event sample according to the measured value of the invariant mass M^{jj} of the two-jet system (326 events have $M^{jj} < 70$ GeV/c^2, 128 have $M^{jj} > 70$ GeV/c^2) shows no significant dependence of $< P_T^{jj} >$ upon M^{jj}.

6.2 - Longitudinal momentum and angular distribution.

The measurement of a limited transverse momentum for two jet systems supports the idea that jets result from the collision of two incident partons, each having a small transverse motion within the colliding hadrons. The longitudinal momentum P_ℓ^{jj} of two-jet systems is, on the contrary, expected to take large values since the colliding partons, depending on the structure functions, may carry very different longitudinal momenta in the initial state.

The measured scattering angles $\theta_{1,2}$ of the jet axes with respect to the beam are related to the rapidity y_{jj} of the two jets and to their

is a measure of the mean shower depth. Figure 13 shows the distribution of X measured for clusters having $E_T > 20$ GeV. This distribution is in good agreement with hadron jets produced in a test beam resulting from the collision of high energy π^-'s with a 10 cm thick polyethylene target but is very different from that measured for single π^-'s [11]. The multi-hadron and single pion distributions of Fig. 13 are evaluated for the energy distribution of the present data using measurements performed with incident π^- and e^- beams of 1 to 70 GeV/c momenta and by means of simple interpolation procedures.

6 - TWO-JET PRODUCTION PROPERTIES

6.1 - Transverse momentum.

It has been shown in Sect. 4 that events having ΣE_T in excess of $\simeq$ 50 GeV are dominated by two-jet topologies, with the jets approximately balancing each other's transverse momentum. The knowledge of the transverse momentum distribution of the two-jet system, P_T^{jj}, provides information about the production mechanism of the jets. The measurement of $\vec{P}_T^{jj}$, the sum of two large and approximately opposite vectors, is sensitive to instrumental effects and requires a good understanding of systematic uncertainties. To extract the initial P_T^{jj} distribution from the observed distribution, a Monte Carlo calculation is made simulating the details of the detector response and generating two-jet events having different P_T^{jj} distributions but having otherwise the same characteristics as observed in the data. We assume that the azimuthal distribution of $\vec{P}_T^{jj}$ is uniform and that its modulus has a distribution of the form $dN/d(P_T^{jj})^2 \propto \exp(-\alpha(P_T^{jj})^2)$ where α is a free parameter related to the mean value of P_T^{jj} via the relation $\alpha = \frac{\pi}{4} < P_T^{jj} >^{-2}$.

The P_T^{jj} distribution is measured in a sample of two-jet events identified as having two clusters with transverse energies in excess of 20 GeV and well contained within the calorimeter acceptance. To avoid favouring small P_T^{jj} events in which both clusters have transverse energies close to 20 GeV we require in addition that the sum of their transverse energies exceed 50 GeV. The same selection criteria are applied to the Monte Carlo sample.

CMS scattering angle θ^*. When $P_T^{jj} \neq 0$, the fraction of P_T^{jj} carried by each of the incident partons is unknown. As a result, in the two jet center of mass system the incident parton momenta are equal and opposite but their angle θ^* with respect to the jet momenta is in principle unknown. We choose to approximate θ^* by the angle between the jet momenta and the external bisector of the p and $\bar{p}$ momenta in the two-jet CMS [23]. The resulting error is negligible when $P_T^{jj} << M^{jj}$. The distribution of $\tanh(y_{jj})$ is shown in Fig. 15 for a sample of two-jet events having $P_T^{jj} < 15$ GeV/c, $M^{jj} > 56$ GeV/c^2 and with $|\cos\theta^*| < 0.3$. As a result of the limited coverage of the central calorimeter ($|\cos\theta_{1,2}| \lesssim 0.7$) the smaller $|\cos\theta^*|$, the larger the $\tanh y_{jj}$ acceptance and, conversely, the smaller $|\tanh(y_{jj})|$, the larger the $\cos\theta^*$ acceptance.

The measured $\tanh(y_{jj})$ distribution of Fig. 15 is consistent with the result of a Monte Carlo calculation assuming a uniform y_{jj} distribution.

The measured $\cos\theta^*$ distribution for events having $|\tanh(y_{jj})| < 0.28$ is shown in Fig. 16. A clear deviation from isotropy (uniform $\cos\theta^*$ distribution) is evidenced [24]. The data are consistent with any of the QCD subprocesses [25] which are expected to have similar $\cos\theta^*$ dependences within the calorimeter acceptance. However the data do not allow disentangling their independent contributions.

7 - ADDITIONAL CLUSTERS AND UNDERLYING EVENT STRUCTURE IN TWO-JET EVENTS

In the present Section we study some properties of the energy density distribution in the angular region which is not covered by the aperture of the two leading jets. We expect this region to be populated partly by the debris of the spectator partons (as predicted by parton models) or initial state gluon bremsstrahlung and partly by particles directly correlated with the leading jets (as suggested from the energy flow analysis presented in Section 5.2).

7.1 - Underlying event structure.

The transverse energy measured in addition to that of the two leading clusters, $\Sigma\tilde{E}_T$, is generally larger than that measured in minimum bias events despite the angular coverage lost to the two main jets. This is illustrated in Fig. 17 where the distribution of $\Sigma\tilde{E}_T$ for two-jet events having $E_T^1 + E_T^2 > 60$ GeV (well above trigger bias) is compared with the ΣE_T distribution of minimum bias events. The mean values of $\Sigma\tilde{E}_T$ and of ΣE_T are 13.1 and 5.5 GeV respectively. The latter decreases to 5.0 GeV when an angular region equal to that covered by two average jet clusters is excluded from the evaluation of ΣE_T. The underlying event has a net transverse momentum ($\Sigma\vec{p}_T$) which partially balances the $\vec{P}_T^{jj}$ of the two-jet system as expected. Conversely, if we exclude from the calculation of $\Sigma\tilde{E}_T$ the third cluster having $E_T > 5$ GeV (if such a cluster is present in the event), the mean value of $\Sigma\tilde{E}_T$ becomes 10.5 GeV, still twice as large as the mean value of ΣE_T measured in minimum bias events. In this case the underlying $\Sigma\vec{p}_T$ has only a very small component balancing the $\vec{P}_T$ of the three-cluster system.

Despite this important difference the transverse energy distributions exhibit similar clustering properties in underlying events and in minimum bias events, as long as they are compared at equal values of $\Sigma\tilde{E}_T$ and ΣE_T. This is shown in Fig. 18 where the average number of clusters exceeding a given threshold is displayed in both cases. The similarity between the two event classes is striking.

The agreement is quantitatively better at high threshold and high $\Sigma\tilde{E}_T$ for the sample in which third clusters exceeding $E_T = 5$ GeV have been excluded.

7.2 - Dalitz diagram of three-cluster events.

Approximately 30% of the events with two leading clusters having $E_T^1 + E_T^2 > 60$ GeV contain an additional cluster with a transverse energy exceeding 4 GeV. To search for a possible structure in the configuration of the three leading jets the corresponding Dalitz diagram for events having $E_T^{1,2} > 15$ GeV and $E_T^1 + E_T^2 + E_T^3 > 60$ GeV is constructed. The energies E_{cm}^i of each of the three leading clusters in their common center of mass system are used to define three quantities $\varepsilon_i = \frac{E^i cm}{M_{jjj}}$, with M_{jjj} being the three-cluster invariant mass. With Q defined as $(2\varepsilon_1 + \varepsilon_2 - 1)/\sqrt{3}$ and the ordering relation $\varepsilon_1 > \varepsilon_2 > \varepsilon_3$ the events populate a triangular domain of the Dalitz plot with corners located at

A : corresponding to two-jet configurations,

B : corresponding to symmetric three-jet configurations with the three jet momenta forming an equilateral triangle,

C : corresponding to three collinear jets.

Figure 19 shows the observed event distribution and its projection on the ε_3 axis. A strong concentration in the vicinity of the two jet region (A) is seen but no other significant structure is observed. On the average 20% of the events contain a third cluster which carries more than 15% of the available energy. Similar conclusions are reached when the analysis is repeated in reduced intervals of M_{jjj}.

7.3 - Additional clusters in two-jet events.

The occasional observation of a third large transverse energy cluster in two-jet events suggests a possible interpretation in terms of gluon bremsstrahlung. However, contrary to the situation in electron-positron collisions, hard gluons may now be radiated also from the initial state partons and/or at the parton scattering vertex. We expect such radiation to be much less correlated with the main jet momenta than in the case of gluons radiated by the final state partons. With this remark in mind we attempt a measurement of the three-jet production rate for configurations in which two of the jet momenta are observed to be correlated.

A sample of two-jet events is selected, each jet having $E_T > 20$ GeV,

in which a third cluster with transverse energy E_T^3 is observed. To avoid an overwhelming contamination of low transverse energy clusters not directly associated with the two jet system, E_T^3 is selected to exceed 4 GeV. While 29% of the initial two-jet sample satisfy this condition (290 events), only 4.5% of minimum bias events contain such a hard cluster. The two main jets are labelled 1 and 2 according to the relation $E_T^1 > E_T^2$ and the angle ω_{13} (ω_{23}) is calculated between the momentum associated with the third cluster and that of jet 1 (2). Distributions in cos ω_{13} and cos ω_{23} are shown in Fig. 20. They exhibit a clear correlation between the third cluster and jet 2, in qualitative agreement with expectation. Imposing a higher E_T^3 threshold enhances this correlation at the price of reducing the event sample. The drops near cos $\omega = \pm 1$ result from the inability of the detector to resolve jets separated by less than about 30° on the average.

In order to evaluate the three-jet production rate the acceptance must be determined and the contribution of uncorrelated third clusters must be subtracted. A Monte Carlo simulation taking into account our detector response is used to generate two-jet or three-jet events onto which the observed energy pattern of minimum bias events chosen at random is superimposed. The observation (see Section 7.1) that similar clustering patterns occur in minimum bias events and in two-jet underlying events at the same ΣE_T justifies this approach for simulation of uncorrelated third clusters. By giving each Monte Carlo event a weight depending upon the $\Sigma \hat{E}_T$ value of the minimum bias event used in its generation, we can generate an arbitrary distribution for $\Sigma \hat{E}_T$. In pratice two extreme cases are considered :

i) underlying events have the same $\Sigma \hat{E}_T$ distribution as minimum bias events,

ii) underlying events have the observed $\Sigma \hat{E}_T$ distribution shown in Fig. 17.

The two-jet and three-jet systems are generated with the same distributions in invariant mass, angle, and longitudinal and transverse momentum. The configuration of the three-jet systems in their CMS is taken to be that of $q\bar{q}g$ final states in e^+e^- collisions [26]. This distribution does not strictly apply to $\bar{p}p$ collisions but should be a sufficient approximation in the kinematic region of interest, where the bremsstrahlung probability is expected to factorize and reduce to the simple parton model

8 - JET PRODUCTION CROSS-SECTION

The measurement of the inclusive production cross-sections

$$\bar{p}p \rightarrow \text{jet} + \text{anything} \qquad (6)$$

$$\bar{p}p \rightarrow \text{jet}_1 + \text{jet}_2 + \text{anything} \qquad (7)$$

can be compared directly with QCD predictions. To the extent that the jets are correctly identified, such comparisons do not require any assumption about the fragmentation mechanism. The leading and next to leading order QCD diagrams describing parton scatterings are expected to provide a good approximation to the production cross-section for large transverse momentum jets.

In the present Section the cross-sections for the processes (6) and (7) as a function of the jet transverse energy (6) and of the two-jet invariant mass (7) are evaluated. The jet direction and energy are taken from the centroid and energy of the cluster seen in the calorimeter as defined using the algorithm discussed above. In forming two-jet invariant masses, the individual clusters are taken to be massless [28].

Events are selected containing at least one cluster with $E_T > 30$ GeV (45 GeV) and events containing at least two clusters with $E_T > 15$ GeV (20 GeV) each from the data accumulated with the low (high) hardware trigger threshold on ΣE_T. In addition the clusters are required to have pseudorapidities η in the interval $-0.85 < \eta < 0.85$ and to have $40^o < \phi < 320^o$. The selected samples contain 1160 events (6) and 1680 events (7). In order to partly account for final state gluon radiation effects discussed in Sect. 7.3, the jet momenta are defined by adding to the measured momentum vector of the selected cluster those of all clusters having $E_T > 3$ GeV and separated by an angle ω from the selected cluster momentum such that $\cos \omega > 0.2$. This increases the observed transverse energy (E_T) distribution for clusters by about 15% roughly independent of E_T.

8.1 - Inclusive jet production.

The evaluation of the inclusive jet production cross section and of the two-jet invariant mass distribution from these events requires the knowledge of the integrated luminosity and the determination of the detector acceptance.

expressions for $q \to qg$ and $g \to gg$ [27]

$$\frac{dR(q \to qg)}{dz\, d(\sin\omega)} = \frac{8\,\alpha_s}{3\pi} \quad \frac{1 - z + 0(z^2)}{z \sin\omega} \qquad (5a)$$

$$\frac{dR(g \to gg)}{dz\, d(\sin\omega)} = \frac{9}{4}\,\frac{8\,\alpha_s}{3\pi} \quad \frac{1 - z + 0(z^2)}{z \sin\omega} \qquad (5b)$$

where R is the bremsstrahlung probability of a gluon carrying a fraction z of the parent parton momentum and emitted at an angle ω to it. The value of the strong coupling constant, α_s, is set to 0.20 in our calculation (which only considers the $q \to qg$ case according to [26]).

The Monte Carlo calculation is used to produce $\cos\omega$ distributions $f_2(\cos\omega)$ and $f_3(\cos\omega)$ corresponding to the two-jet and three-jet hypotheses. In each case the two extreme configurations mentioned earlier for the underlying event (identical to that of minimum bias events, $f_{2,3}^{mb}$, or enhanced towards large values of $\Sigma\tilde{E}_T$, $f_{2,3}^{enh}$) are considered. No significant difference is observed between f_3 and f_3^{enh}, indicating that the $\cos\omega$ distribution of three jet events is insensitive to the underlying event configuration.

A good description of the observed $\cos\omega$ distribution (Fig. 20) is obtained using a form $\lambda\, f_2^{enh} + (1-\lambda)\, f_2^{mb} + \mu\, f_3$. The data favour $\lambda = 1$, $\mu = 0.8$, but a good fit is also obtained with $\lambda = 0$, $\mu = 1.2$: more data are needed to disentangle with sufficient accuracy the underlying event contribution. Nevertheless, in both cases, the Monte Carlo calculation provides a fair description of the energy distribution of the third cluster and can be used as a convenient model to evaluate the acceptance correction to the bremsstrahlung probability measurement.

Defining as $\mathcal{P}$ the probability that the event contains a third jet correlated to jet 2 in the region $0.2 < z < 0.5$, $0.25 < \cos\omega < 0.75$, we find $\mathcal{P} = 0.22 \pm 0.06$.

The region in (z, $\cos\omega$) is chosen to ensure good acceptance. The quoted error is mostly systematic and includes the uncertainty attached to our knowledge of the contribution of uncorrelated clusters.

The number of events in the data sample is not sufficient to allow a measurement of a possible dependence of $\mathcal{P}$ on the three-jet invariant mass.

The integrated luminosity is obtained by counting the total number of minimum bias events that occured during data taking. It amounts to $\int \mathcal{L} dt = 15.1\ nb^{-1}$. We assign an uncertainty of ±20% to this value from the fluctuations observed during different running conditions and from the overall uncertainty in the cross section accepted by our minimum bias trigger [12]. The loss in the observed E_T distribution resulting from the requirement of a pair of small angle charged secondaries in coincidence with the large ΣE_T trigger was measured in special runs where this condition was disabled from the trigger. The loss is < 5% (90% confidence level) for $\Sigma E_T > 40$ GeV.

The acceptance is calculated using a Monte Carlo simulation of the detector. The Monte Carlo events are processed through the same analysis chain as the data. The simulation reproduces the details of the event configuration and of the detector response, using the same weighting factors for the three calorimeter compartment energies as for the data (Section 3.2). In particular, the distribution of cluster size (Fig. 10) and both hadronic fragmentation and shower development are adequately described. The comparison of the E_T distribution of the Monte Carlo clusters with that of the partons used as input provides the acceptance function $\varepsilon(E_T)$ by which the observed cross-section must be divided to obtain the jet inclusive cross-section. The function $\varepsilon(E_T)$ varies from 0.6 to 0.8 over the range $30 < E_T < 100$ GeV. It accounts for both the limited solid angle coverage of the detector (Fig. 1), and the jet energy measurement errors. Varying relevant analysis parameters, such as the rapidity range accepted, the parameters of the clustering algorithm, and the relative weights attributed to the energy depositions in the various calorimeter compartments affects both the observed E_T distribution and $\varepsilon(E_T)$ but the corrected cross-sections do not change by more than 15%.

Uncertainties in the details of the jet fragmentation contribute further systematic errors to $\varepsilon(E_T)$, the main effect being a change of the energy scale. The effect is estimated to be less than 15% by comparing Monte Carlo events obtained with different fragmentation models.

The cross-section for inclusive jet production $d^2\sigma/dE_T d\eta$ at $\eta = 0$ is shown in Fig. 21 as a function of the jet transverse energy E_T and listed in Table 1. The quoted errors include the statistical errors and the energy dependent systematic uncertainty of $\varepsilon(E_T)$. A systematic normalization uncertainty of ±25% in the cross section scale (with contributions

from the total integrated luminosity and from the acceptance calculation) as well as a ±6% uncertainty in the E_T scale (due to the calorimeter calibration, the response to hadrons [11], the cluster algorithm, and variations in fragmentation models used in the Monte Carlo) have to be added. As already mentioned the contribution of events from sources other than $\bar{p}p$ collisions is estimated from a visual scan to be < 5%, independent of E_T. The resulting overall systematic uncertainty in the inclusive jet cross-section is about ±40%.

The present result is obtained from a data sample about 200 times larger than the one available at the time of our first observation [5] of jet production at the $\bar{p}p$ collider. The present cross-section (Fig. 21) is larger than that reported then, the main improvement being a refined knowledge of the energy scale. The result is at a level comparable with QCD calculations [20,29,30] as shown in Fig. 21. The cross-section joins smoothly the measurements of UA1 [6] and they agree in the region of overlap.

The rms energy resolution in the region around E_T = 40 GeV is about ±5 GeV. No evidence for statistically significant structure is seen in Fig. 21. From a fit to the data with the form $d^2\sigma/dE_T d\eta \propto AE_T^{-n}$ we obtain $A = (4.7 \pm .3).10^{12}$ nb GeV^{-1}, $n = 7.2 \pm 0.2$ with a χ^2 of 15 for 21 degrees of freedom.

8.2 - Isolated neutral particles.

Also shown in Fig. 21 (open circles) is the cross section for the production of large transverse momentum single isolated neutral particles (γ, π^0, η, ...), identified using the pre-shower counter (C5) in front of the electromagnetic calorimeter. The events contributing to the cross section shown are selected using a procedure quite similar to that used to search for high transverse momentum electrons [31], but requiring that no track face a highly electromagnetic cluster (the energy of the hadron compartments must be less than 10% of the cluster energy). To ensure that the cluster is from an isolated single particle, signals in C5 consistent with no more than two photons converting in the tungsten converter are required. The resulting sample of 51 events yields a cross section for single isolated neutral particles that is expected to be a factor 2-3

smaller [32] than the corresponding inclusive cross section. By studing the distribution of the number of photons converted, the contribution of single π^0 and single γ can be estimated : the data of Fig. 21 are consistent with being all from π^0 but the ratio γ/π^0 could be as large as 35% (at 90% confidence level). The error bars shown are statistical only, systematic uncertainties contribute and additional ±30%, independent of the transverse energy, to the uncertainty in the overall normalization.

8.3 - Two-jet mass distribution.

Figure 22 shows the distribution of the invariant two-jet mass (M_{jj}) for events containing two jets each having $E_T > 20$ GeV and lying within $-.85 < \eta < .85$. The errors shown are statistical only. There are additional systematic uncertainties arising from the same sources as discussed in Section 8.1 for the inclusive jet cross section. The normalization uncertainty is ±40% which includes the uncertainty on the mass scale of ±6%. The rms mass resolution in the region of 80 GeV/c^2 is $\sim$ ±8 GeV/c^2. On the basis of the observed $W \to e\nu$ events in the central calorimeter [31], we expect in this mass region about 15 events originating from the production of the intermediate vector bosons ($W^{\pm}$, Z^0) and their subsequent decay into two-jet final states. However, no evidence for significant structure is seen : with the present statistics, the signal is expected to be hidden by the large background of continuum two-jet production. In the mass range $60 < M_{jj} < 220$ GeV/c^2, the data fit a form $d\sigma/dm_{jj} \propto Ae^{-bM_{jj}}$ with A = 586 ± 85 nb GeV$^{-1}c^2$, b = (6.6 ± 0.2)·10^{-2} GeV$^{-1}c^2$ and with a χ^2 of 17 for 17 degrees of freedom.

9 - CONCLUSIONS

This paper has presented a summary of the production and properties of jets at the CERN $\bar{p}p$ collider. The observation [5] that events in $\bar{p}p$ collisions at $\sqrt{s}$ = 540 GeV with large transverse energy in a rapidity interval of two units around 90^{o} have a dominant two-jet structure has been confirmed with much higher statistics. Detailed studies of the fragmentation properties of these jets have begun. In particular, the charged particle multiplicities have been measured as a function of the jet energy. The production of isolated neutral particles has been observed and found to be about 10^{-3} of the jet yield. The production properties of the two-jet system have been measured : its mean transverse momentum is limited with a value of about 5 GeV/c and its rapidity distribution is consistent with being uniform within our acceptance while the distribution of the center of mass scattering angle shows a clear peaking towards small angles as expected for parton scattering. Production of additional energy clusters in two-jet events has been observed and found to be consistent with expectation for final state gluon bremsstrahlung processes, but higher statistics are needed for more detailed studies. The inclusive jet production cross section and the two-jet invariant mass distribution are at a level comparable with QCD calculations. No significant structure in the jet-jet mass plot is seen up to masses of 150 GeV/c^2.

ACKNOWLEDGEMENTS

This experiment would have been impossible without the collective effort of the staffs of the relevant CERN accelerators, whom we gratefully acknowledge.

We deeply thank the technical staffs of the Institutes collaborating in UA2 for their invaluable contributions. We are particularly indebted to C. Bruneton, D. Burkhart, W. Carena, J-P. Dufey, F. Gagliardi, H. Grote, D. Klein, M. Mermikides, G. Mornacchi, B. Nilsson, M. Sciré, D. Sendall, A. Silverman, A. Vascotto and V. White for their contributions to the on-line data acquisition system and to the data analysis, to G. Bertalmio, G. Bosc, F. Bourgeois, M. Dialinas, G. Dubail, A. Hrisoho, C. Lamprecht, F. Impellizzeri, G. Reiss, B. Rossini, P. Wicht and their teams for major contributions to the construction of the detector and to L. Bonnefoy, J-M. Chapuis, Y. Cholley, G. Dubois-Dauphin, G. Gurrieri, M. Hess, G. Iuvino, M. Lemoine, A. Sigrist, G. Souchère and A. Vicini for their invaluable technical contribution.

We are grateful to the UA4 collaboration for providing the signals from the small-angle scintillator arrays.

We thank M. Holder and G. Wolf from the TASSO Collaboration and B. Eckart from the UA5 Collaboration for communicating to us unpublished data. We have enjoyed many fruitful discussions with colleagues from the theory departments, in particular we would like to thank A.P. Contogouris, R. Horgan, B. Humpert, G. Ingelman, M. Jacob, S. Kunszt and B.R. Webber.

We thank H.H. Williams for his stimulating contributions to the early phase of this experiment.

Special thanks are due to M. Prost and E. Vial for their invaluable help in editing this article.

Financial supports from the Schweizerischer National-fonds zur Fördering der Wissenschaftlichen Forschung to the Bern group, from the Danish Natural Science Research Council to the Niels Bohr Institute group, from the Institut National de Physique Nucléaire et de Physique des Particules to the Orsay group, from the Istituto Nazionale di Fisica Nucleare to the Pavia group, and from the Institut de Recherche Fondamentale (CEA) to the Saclay group are acknowledged.

REFERENCES

[1] R.P. Feynman, Photon Hadron Interactions, Benjamin, New York, 1972 ; S.M. Berman and M. Jacob, Phys. Rev. Lett. 25 (1970) 1683 ; S.M. Berman, J.D. Bjorken and J.B. Kogut, Phys. Rev. 4D (1971) 3388.

[2] For reviews see for example : Jets in High Energy Collisions, Physica Scripta 19 (1979), edited by K. Hansen and P. Hoyer ; P. Darriulat, Ann. Rev. Nucl. Part. Sci. 30 (1980) 159.

[3] B. Alper et al., Phys. Lett. 44B (1973) 521 ; M. Banner et al., Phys. Lett. 44B (1973) 537 ; F.W. Büsser et al., Phys. Lett. 46B (1973) 471.

[4] M.G. Albrow et al., Nucl. Phys. B160 (1979) 1 ; A.L.S. Angelis et al., Phys. Scripta 19 (1979) 116 ; A.G. Clark et al., Nucl. Phys. B160 (1979) 397 ; D. Drijard et al., Nucl. Phys. B166 (1980) 223.

[5] The UA2 Collaboration, M. Banner et al., Phys. Lett. 118B (1982) 203.

[6] The UA1 Collaboration, G. Arnison et al., Phys. Lett. 123B (1983) 115.

[7] The Axial Field Spectrometer Collaboration, T. Åkesson et al., Phys. Lett. 118B (1982, 185 and 193 ; A.L.S. Angelis et al., CERN-EP-83-46 (1983) accepted for publication in Phys. Lett. B.

[8] G. Wolf, Proceedings of the 21st Int. Conf. on High Energy Physics, Journal de Physique, supp. 12, tome 43, colloque C-3, Dec. 1982.

[9] The Staff of the CERN $\bar{p}p$ Project, Phys. Lett. 107B (1981) 231.

[10] The UA2 Collaboration, M. Banner et al., Phys. Lett. 115B (1982) 59 and 122B (1983) 322.

[11] The Central Calorimeter of the UA2 Experiment at the CERN $\bar{p}p$ Collider A. Beer et al., to be published in Nucl. Instrum. Methods.

[12] The cross-section seen by the "minimum bias" trigger counters amounts to 43.9 ± 3.5 mb as measured by :

The UA4 Collaboration, R. Battiston et al., Phys. Lett. 117B (1982) 126 and contribution to the XVIII Rencontre de Moriond on Proton-Antiproton Collider Physics, La Plagne, March 19-25, 1983 (to be published).

[13] C. de Marzo et al., Phys. Lett. 112B (1982) 173 ;
M. Arenton et al., Evidence for jets from a transverse energy triggered calorimeter experiment at FERMILAB, Contrib. XXIst Intern. Conf. on High Energy Physics (Paris, France, July 1982) ;
B. Brown et al., Properties of high transverse energy hadronic events, NAL preprint FERMILAB-Conf.-82/34 (Exp. 1982).

[14] The UA5 Collaboration, K. Alpgård et al., Phys. Lett. 115B (1982) 71, and B. Eckart private communication.

[15] The TASSO Collaboration, R. Brandelik et al., Phys. Lett. 86B (1979) 243 and 89B (1980) 418 and private communication from M. Holder and G. Wolf.

[16] B.R. Webber, Contribution to the XVIII Rencontre de Moriond on Proton-Antiproton Collider Physics, La Plagne, March 19-25, 1983 and CERN TH-3569 (1983).

[17] Compiled in : G. Wolf, High energy e^+e^- interactions, DESY 81-086 (1981) ;
R. Plunkett, PhD Thesis Cornell University (1983).

[18] A.G. Clark et al., op. cit.

[19] G. Sterman and S. Weinberg, Phys. Rev. Lett. 39 (1977) 1436.
K. Shizuya and S-H. H. Tye, Phys. Rev. Lett. 41 (1978) 787.
M.B. Einhorn and B.G. Weeks, Nucl. Phys. B146 (1978) 445.

[20] R. Horgan and M. Jacob, Nucl. Phys. B179 (1981) 441.

[21] ISAJET programme, written by F. Paige and S. Protopopescu, BNL report 31987 (1981).

[22] R.D. Field and R.P. Feynman, Nucl. Phys. B136 (1978) 1.

[23] J.C. Collins and D.E. Soper, Phys. Rev. D16 (1977) 2218.

[24] Measurements of angular distributions from leading jet fragments can be found in :
A.L.S. Angelis et al., Nucl. Phys. B209 (1982) 284 ;
D. Drijard et al., Phys. Lett. 121B (1983) 433.

[25] B.L. Combridge, J. Kripfganz and J. Ranft, Phys. Lett. 70B (1977) 234.

[26] T.A. de Grand, Y.G. Ng and S.H.H. Tye, Phys. Rev. D16 (1977) 3251 ;
J. Ellis, M.K. Gaillard and G.G. Ross, Nucl. Phys. B111 (1976) 253.

[27] G. Altarelli and G. Parisi, Nucl. Phys. B126 (1977) 298.

[28] J.D. Bjorken, Phys. Rev. D8 (1973) 4098.

[29] B. Humpert, private communication.
The curves shown on Figs. 21 and 22 were calculated with $\Lambda = 0.5$ GeV, $Q^2 = 2\hat{s}\hat{t}\hat{u}/(\hat{s}^2 + \hat{t}^2 + \hat{u}^2)$ and parametrizations for the structure functions according to (curve A) the counting rule parametrization of J. Owens and E. Reya, Phys. Rev. D17 (1978) 3003 or (curve B) R. Baier et al., Zeitschr. f. Physik C, 2 (1979) 265 ;
B. Humpert, in preparation.

[30] W. Furmanski and H. Kowalski, CERN-EP/83-21 (1983) ;
N.G. Antoniou et al., LPTHE Orsay 83/4, and Phys. Lett. B (in press);
Z. Kunszt and E. Pietarinen, Ref. TH-3584 CERN (1983).

[31] The UA2 Collaboration, M. Banner et al., Phys. Lett. 122B (1983) 476.

[32] G. Ingelman, private communication.

TABLE 1

Inclusive cross section for $\bar{p}p \to$ jet + X at $\sqrt{s}$ = 540 GeV.

E_T (GeV)	$\frac{d^2\sigma}{dE_T\,dy}\Big\vert_{y=0}$ (nb GeV^{-1})
31	53.5 ± 13.0
33	35.1 8.2
35	28.5 6.5
37	19.7 4.5
39	12.0 2.9
41	9.0 2.3
43	9.4 2.3
45	4.46 0.81
47	3.16 0.58
49	1.96 0.38
51	1.70 0.33
53	1.41 0.28
55	1.12 0.24
57	0.77 0.17
59	0.82 0.19
62	0.63 0.12
66	0.198 0.057
70	0.235 0.062
74	0.122 0.043
78	0.080 0.034
86	0.021 0.010
98	0.012 0.007
110	0.008 0.005

The listed errors include the statistical and the E_T-dependent systematic uncertainties. The additional overall systematic error on $d^2\sigma/dE_T dy$ (y = 0) is ±40% (see text).

FIGURE CAPTIONS

1 - Schematic detector assembly :
   a) longitudinal cut parallel to the beam,
   b) transverse cut through the beam.

2 - Observed total transverse energy ΣE_T distribution.

3 - a) The fractions h_1 and h_2 of the total transverse energy ΣE_T contained in the cluster, and respectively the two clusters, having the largest E_T are displayed versus ΣE_T.
   b) Dependence on ΣE_T of the ratios $r_{21} = E_T^2/E_T^1$ and $r_{32} = E_T^3/E_T^2$ (see text).

4 - Azimuthal separation $\Delta\phi_{12}$ between the two largest clusters having $E_T > 20$ GeV for events with $\Sigma E_T > 60$ GeV.

5 - Configuration of the event with the largest ΣE_T, 213 GeV.
   a) cell transverse energy distribution as a function of polar angle θ and azimuth ϕ,
   b) transverse display of the calorimeter and vertex detector.

6 - Azimuthal separation $\Delta\phi$ between the energy cluster centroid of jet E_T^1 and all charged transverse vertex tracks.

7 - Mean charged particle multiplicities in jets n_{ch}^{jet} as a function of $\sqrt{s_{e^+e^-}}$ for e^+e^- and of the invariant two-jet mass M_{jj} for $\bar{p}p$.
   a) lower bound on n_{ch}^{jet},
   b) corrected values of n_{ch}^{jet} for $\bar{p}p$ data.
   See text for details ; the data are compared to results from Refs. (15, 17, 18).

8 - Distribution of the azimuthal transverse energy density $dE_T/d\,\Delta\phi$, where $\Delta\phi$ is measured with respect to the centroid of the highest E_T cluster. The results are shown separately for three ranges of E_T.

9 - Distribution of the normalized energy density $1/E\ (dE/d\psi^2)$ for two intervals of the cluster energy E.

10 - Jet aperture distribution for a sample of two jet events having $E_T^1 + E_T^2 > 40$ GeV (black circles).
Monte Carlo predictions using fragmentation models with $\frac{dN}{dq_T{}^2} \propto e^{-\lambda q_T{}^2}$ (curve a) or allowing for a previous bremsstrahlung (curve b) are shown for comparison (see text). In both cases the variations achieved by allowing for reasonable changes of the relevant parameters are indicated by cross-hatched bands.

11 - a) Uncorrected p_T distribution for charged particles in the jet for data (dots) and Monte Carlo (curve).
b) Fraction of jet energy carried by charged particles for uncorrected data (dots) and Monte Carlo (curve).

12 - Distribution of the observed transverse momentum squared of jet fragments relative to the jet axis (q_T^2) for data (dots) and Monte Carlo simulations with gluon bremsstrahlung (curve).

13 - The distribution of the quantity $X = E_{em}/(E_{em} + E_{H1})$, related to the mean shower depth, for clusters having $E_T > 20$ GeV
- as measured in a sample of two jet events (black circles),
- as measured for incident π^-'s in the same energy range (dotted line),
- as measured for hadron jets produced in a test beam in the same energy range (black curve).

14 - a) Definition of the (ξ, η) coordinate system in the transverse plane.
b,c) The distributions of p_ξ^{jj} and p_η^{jj} (black circles) for a sample of two-jet events are compared with the result of a Monte Carlo calculation using $< p_T^{jj} > = 5$ GeV/c. Horizontal arrows indicate measurement distortions of instrumental origin (see text).

15 - Uncorrected distribution of $\tanh(y_{jj})$. The curve shows the result of a Monte Carlo calculation with a uniform y distribution.

16 - Uncorrected CMS scattering angle distribution. The dashed curve is the result of a Monte Carlo calculation for a uniform $\cos\theta^*$ distribution whereas the solid curve shows the prediction for $gg \to gg$ scattering (arbitrary normalization).

17 - Uncorrected transverse energy distributions for a sample of minimum bias events and underlying events in two - or three -jet configurations (see text).

18 - Mean cluster multiplicities, shown for clusters above several different thresholds, in minimum bias events and in underlying events in two - or three -jet configurations (see text).

19 - Three-jet Dalitz diagram and its projection onto the ε_3 axis (observed data, no acceptance correction, see text).

20 - Angular correlation in three-jet events. Here $\cos\omega$ is defined as $\cos\omega = \cos\omega_{23}$ if $\cos\omega_{23} > 0$ and $\cos\omega = -\cos\omega_{13}$ if $\cos\omega_{13} > 0$. Best fits to the data (black circles) are presented for two underlying event configurations :
a) ΣE_T distribution as in Fig. 17,
b) ΣE_T distribution as for minimum bias events.

21 - Inclusive jet production cross section. The additional systematic uncertainty is ±40%. Curves A and B are predictions from QCD calculations [29] using different parametrizations for the structure functions. The open points correspond to single isolated neutral particles (see text).

22 - Two-jet production cross section in the pseudo-rapidity range $-0.85 < \eta < 0.85$. The additional systematic uncertainty is ±40%. (curves as for Fig. 21).

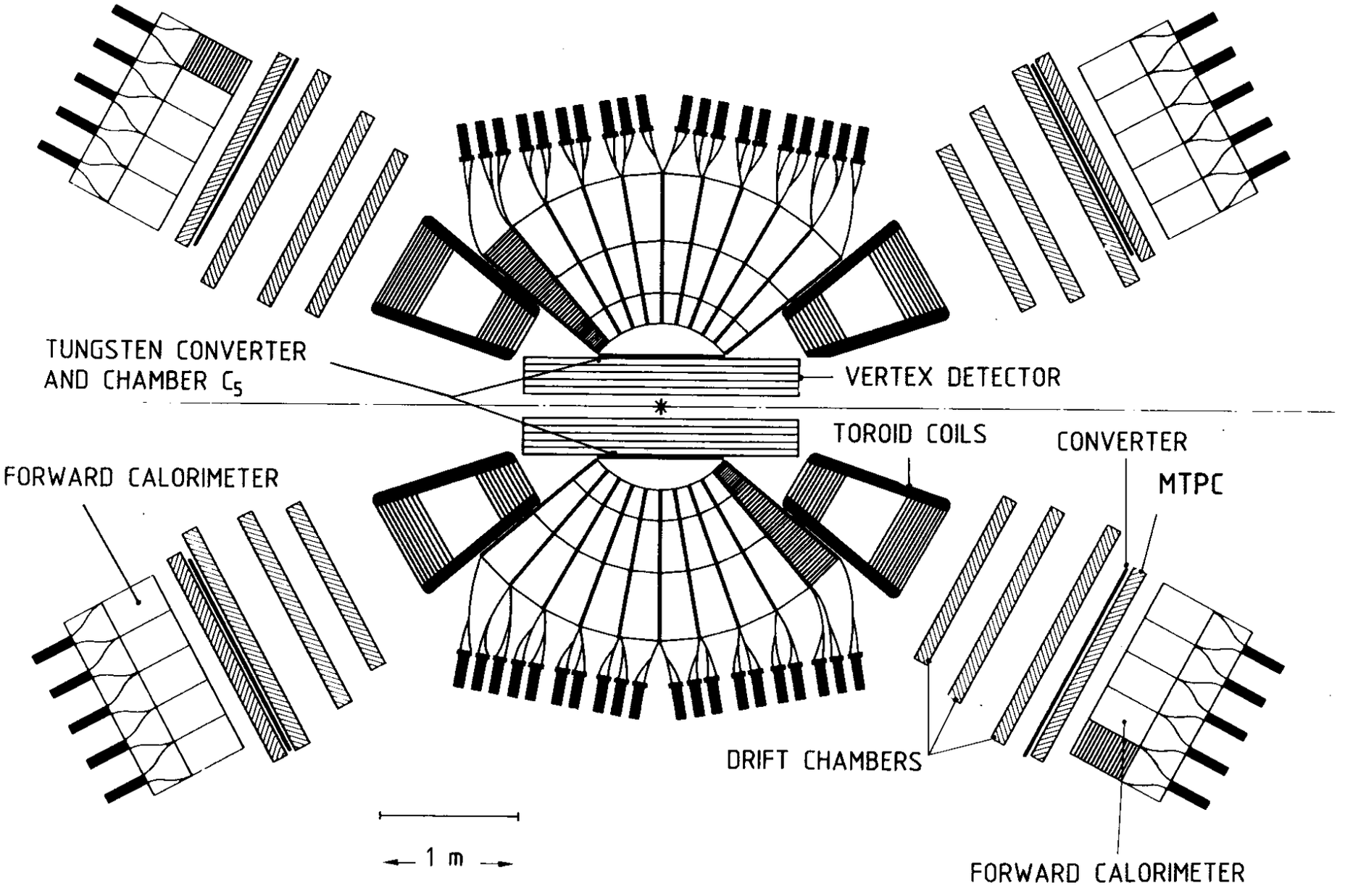
TUNGSTEN CONVERTER
AND CHAMBER C_5
VERTEX DETECTOR
TOROID COILS
CONVERTER
MTPC
FORWARD CALORIMETER
DRIFT CHAMBERS
1 m
FORWARD CALORIMETER

Fig. 1 a

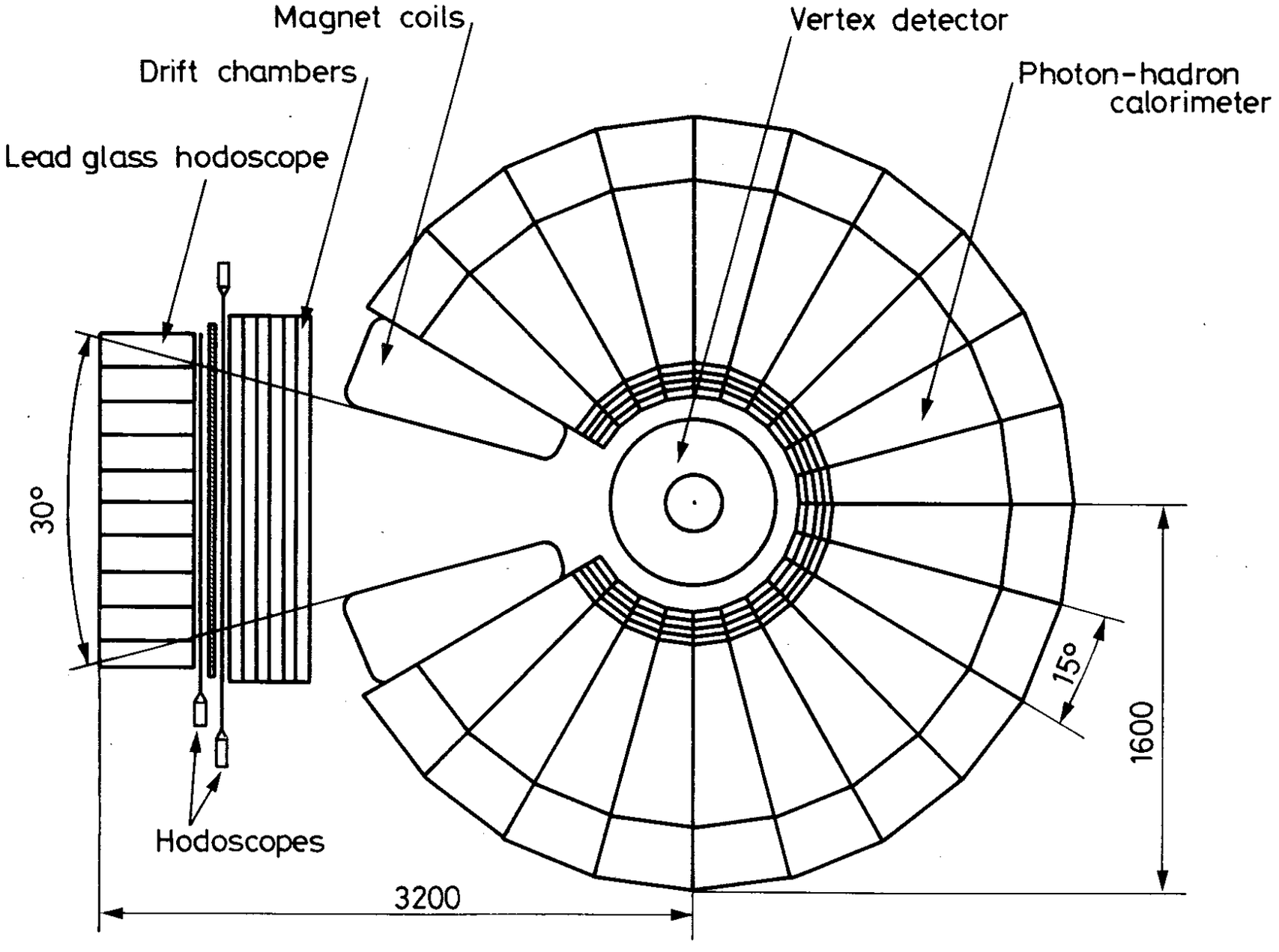
Magnet coils
Vertex detector
Drift chambers
Photon-hadron calorimeter
Lead glass hodoscope
30°
15°
1600
Hodoscopes
3200

Fig. 1 b

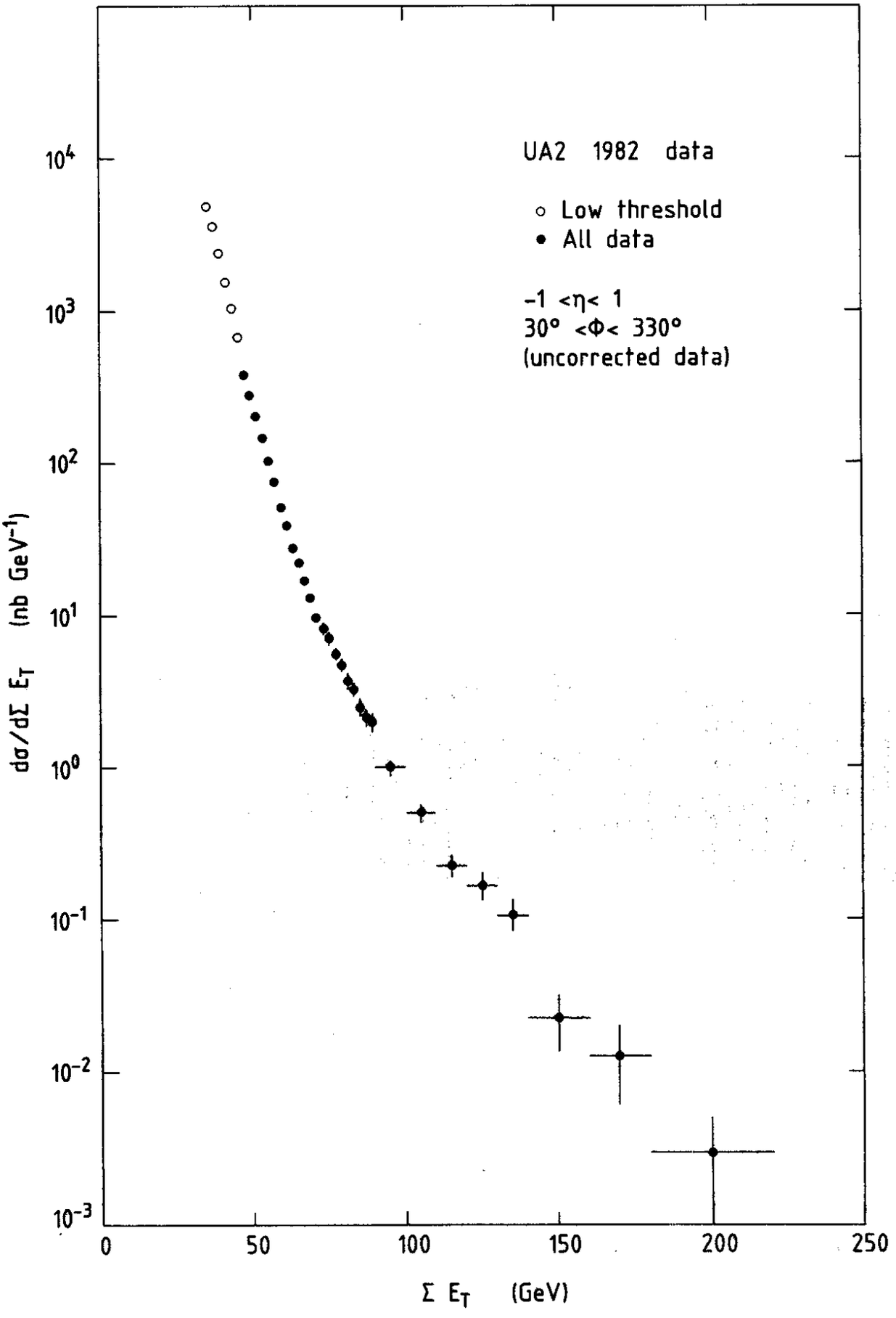
UA2 1982 data
○ Low threshold
● All data
-1 <η< 1
30° <Φ< 330°
(uncorrected data)
dσ/dΣ E_T (nb GeV^-1)
Σ E_T (GeV)
10^4
10^3
10^2
10^1
10^0
10^-1
10^-2
10^-3
0
50
100
150
200
250

Fig. 2

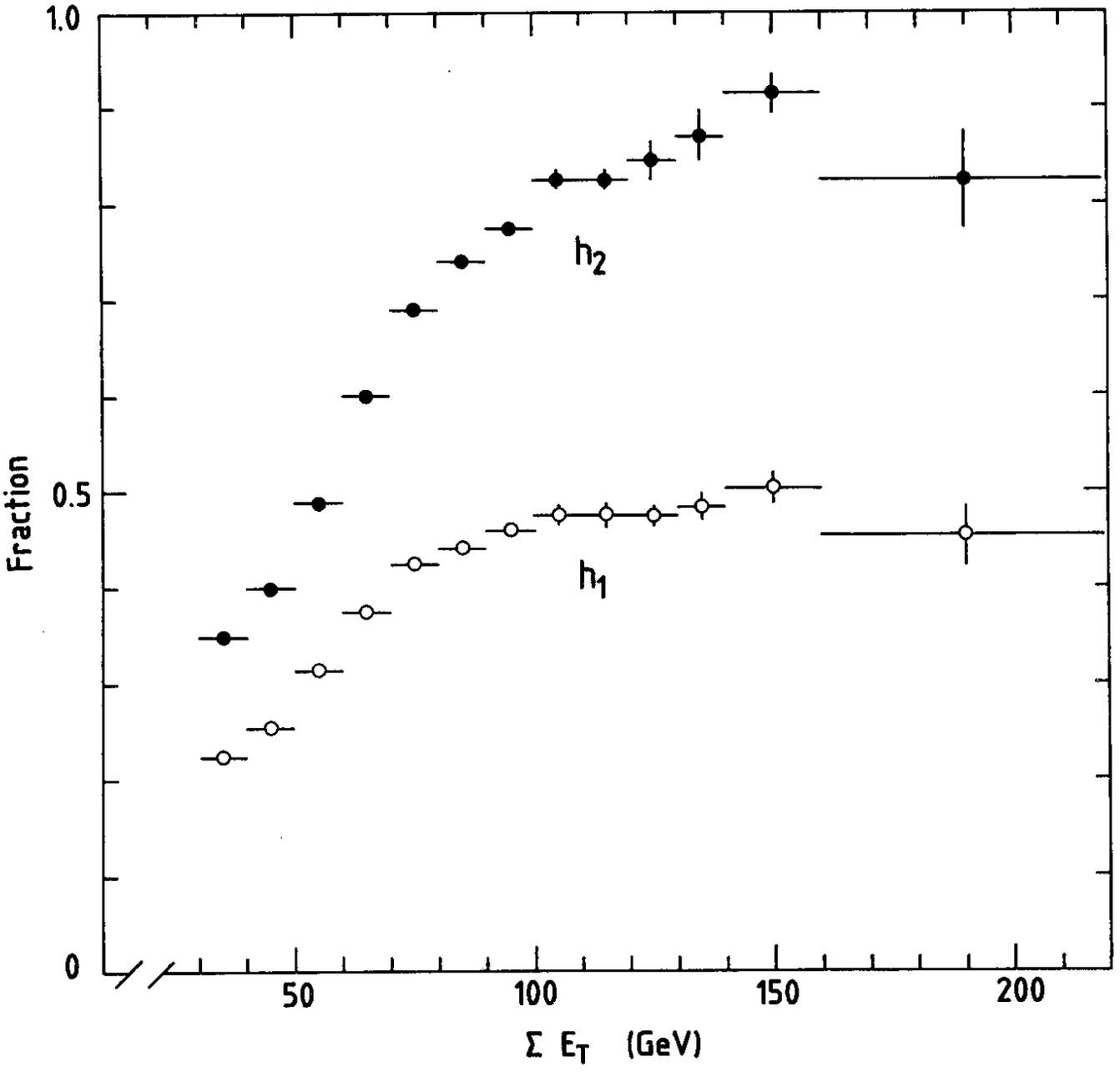

Fig. 3 a

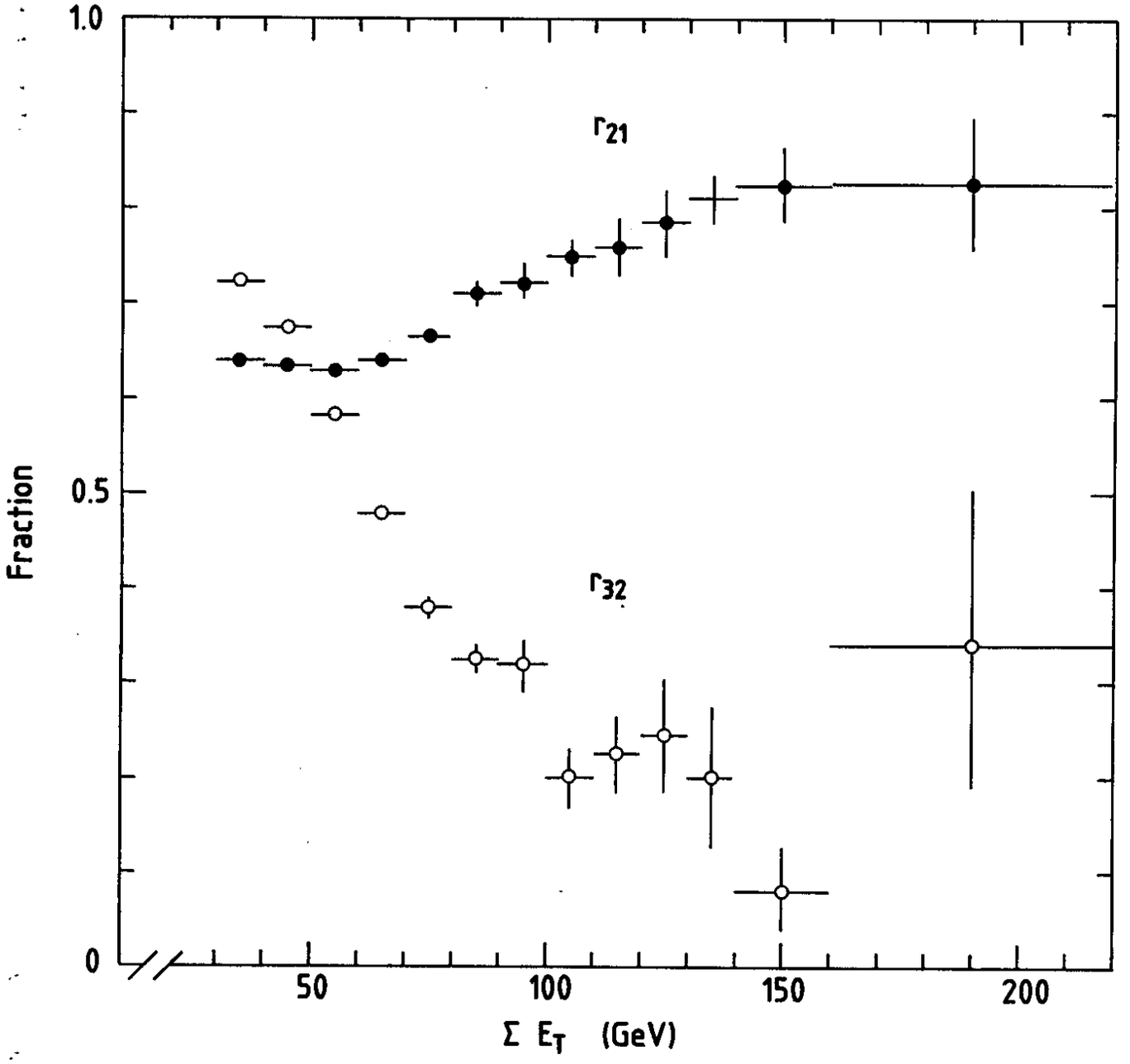

Fig. 3 b

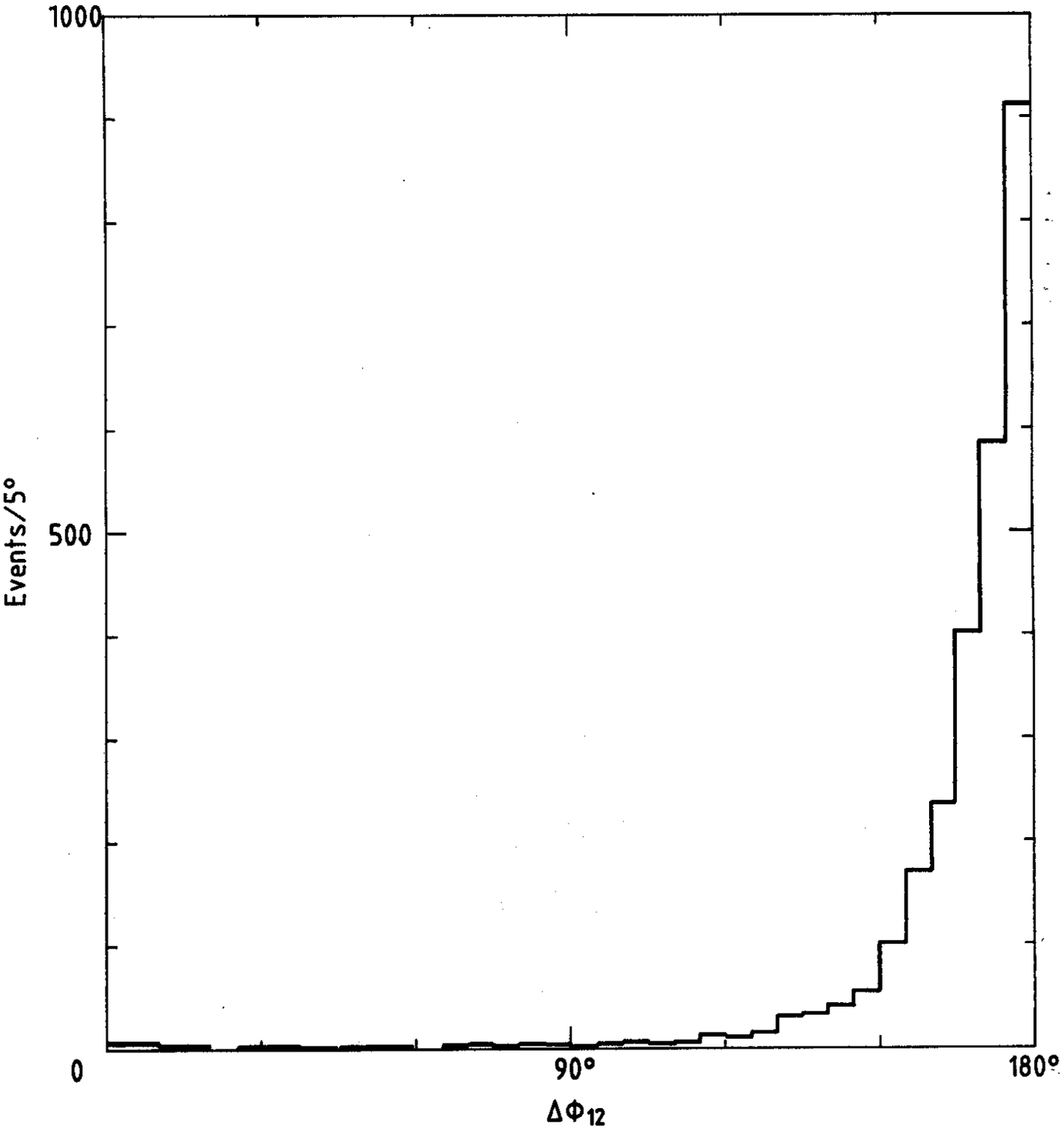

Fig. 4

TRANSVERSE ENERGY DEPOSITION

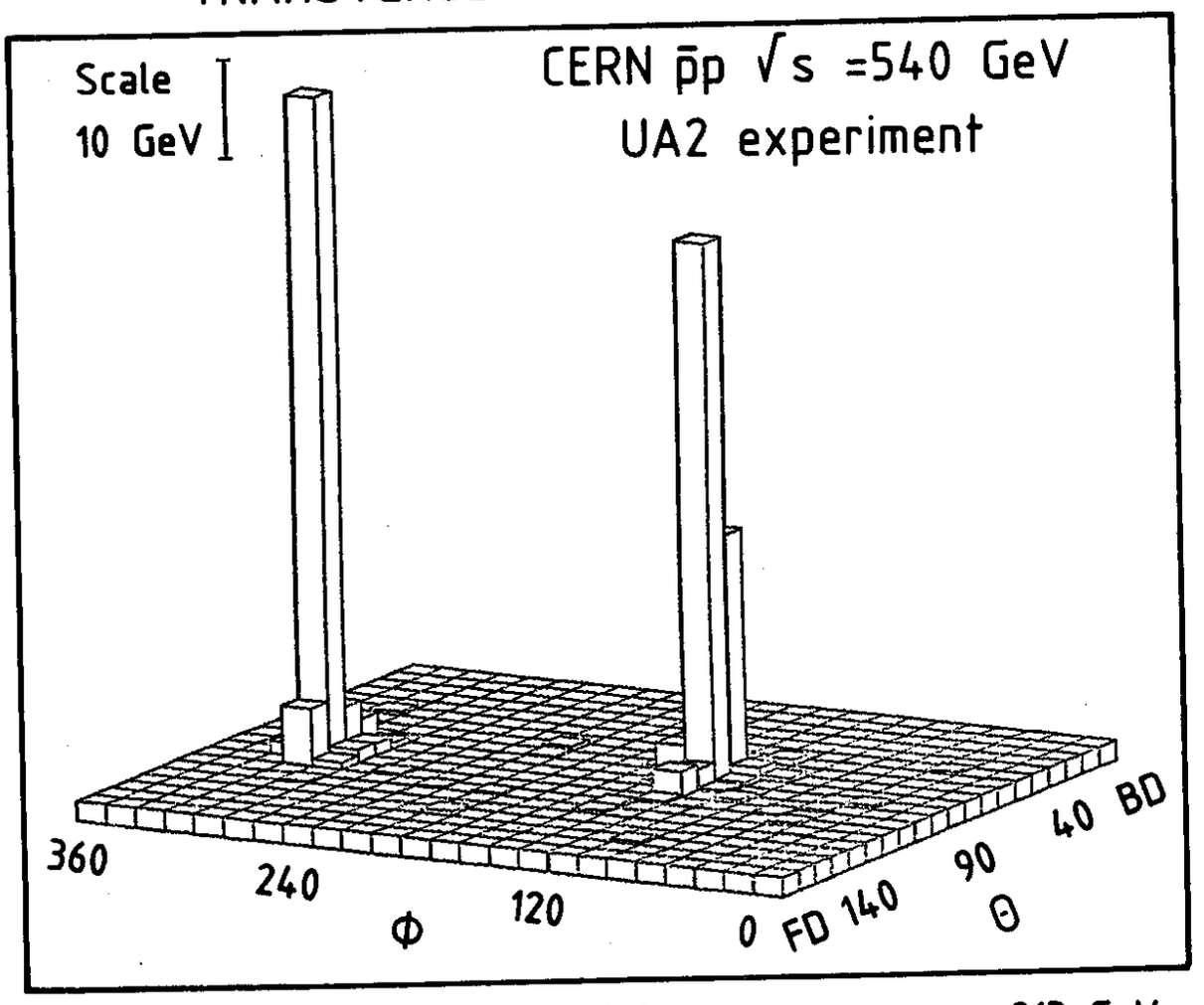

Run NO. 1465
Trigger NO. 43978

Total transverse energy 213 GeV

Fig. 5 a

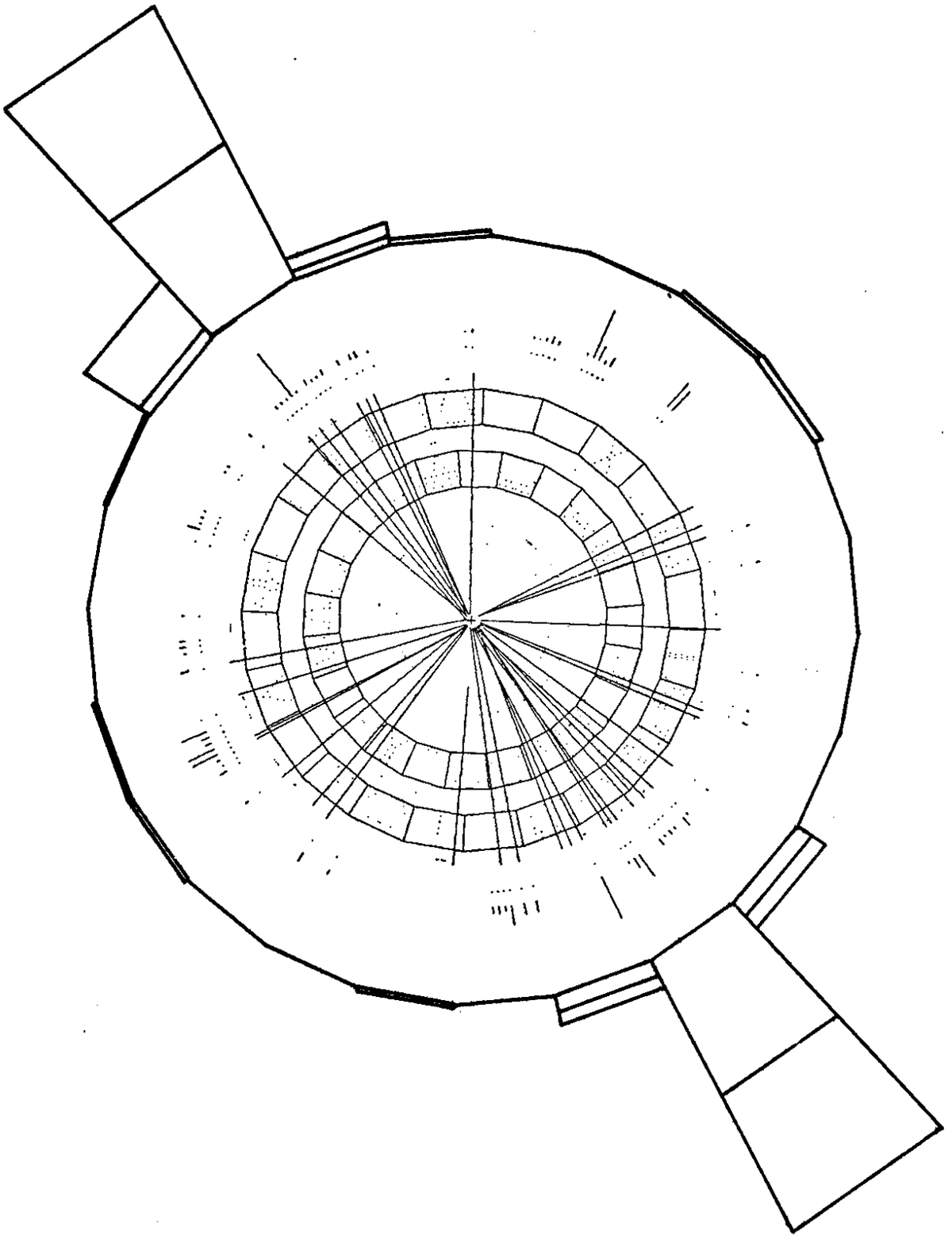

Fig. 5 b

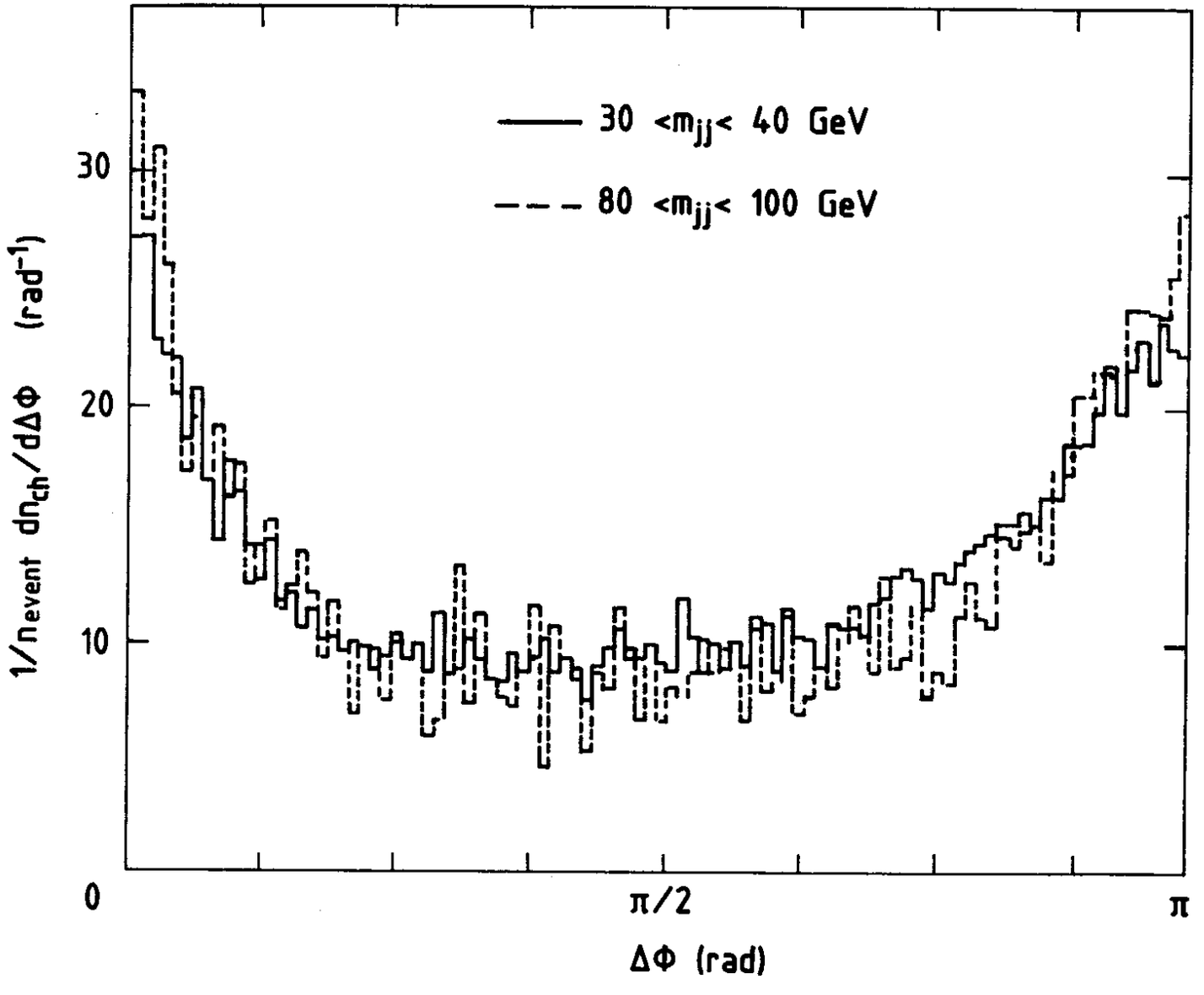
30 <m_jj< 40 GeV
80 <m_jj< 100 GeV
1/n_event dn_ch/dΔΦ (rad^-1)
30
20
10
0
π/2
π
ΔΦ (rad)

Fig. 6

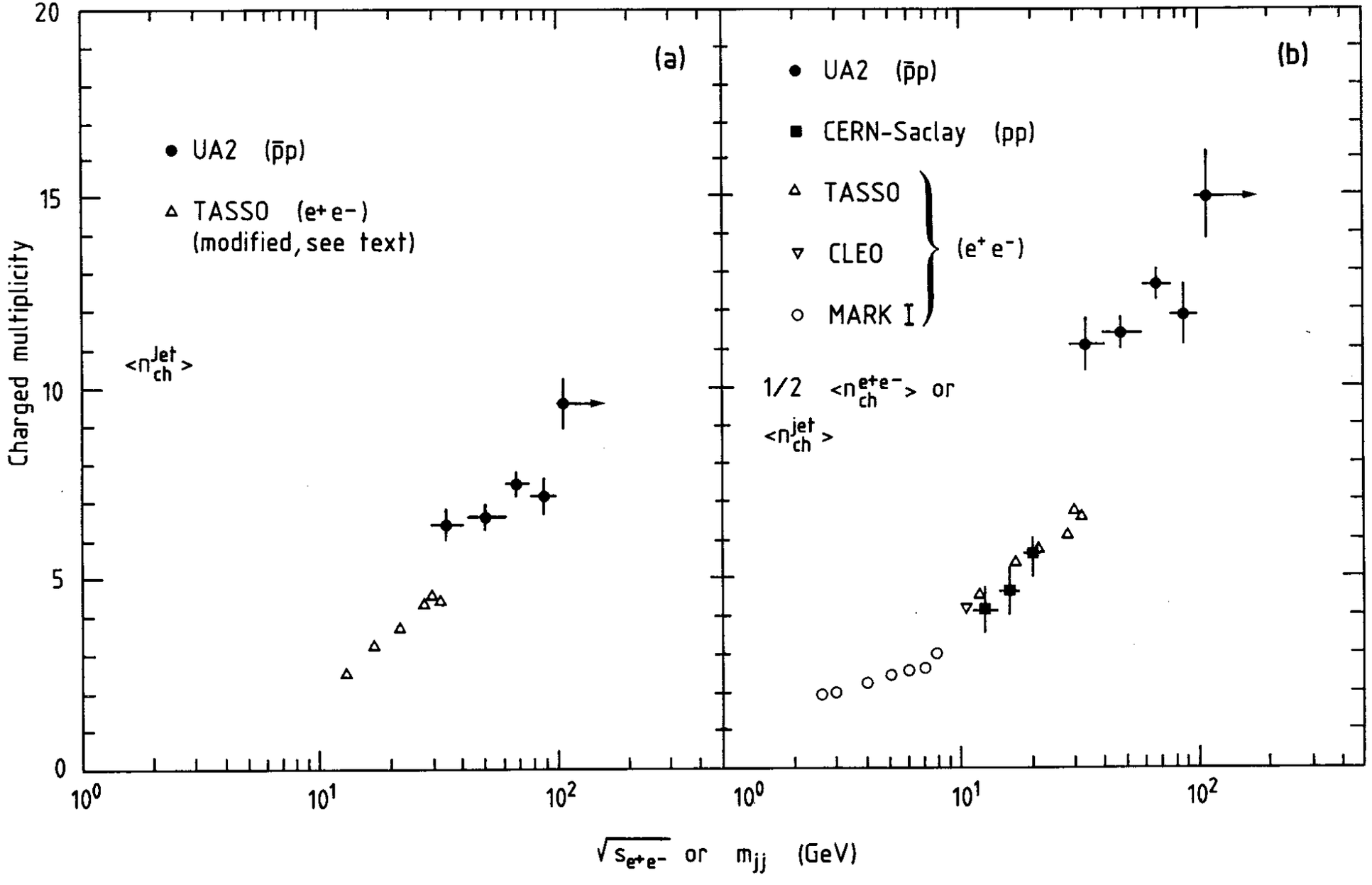
(a)
(b)
UA2 (p̄p)
TASSO (e+e−)
(modified, see text)
CERN-Saclay (pp)
TASSO
CLEO
MARK I
(e+e−)
<n_ch^jet>
1/2 <n_ch^e+e−> or
<n_ch^jet>
Charged multiplicity
√s_e+e− or m_jj (GeV)
0
5
10
15
20
10^0
10^1
10^2

Fig. 7

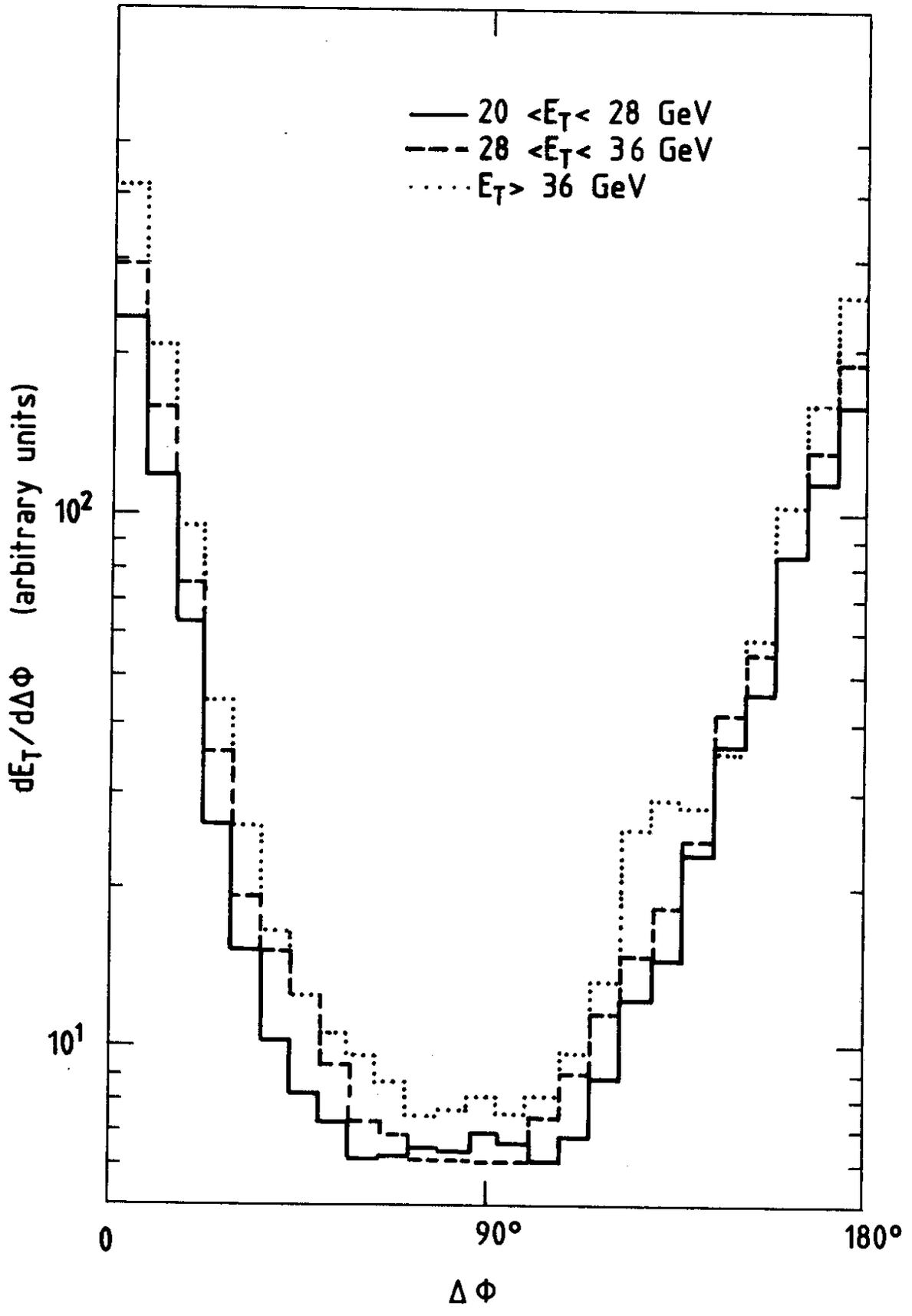
20 <E_T< 28 GeV
28 <E_T< 36 GeV
E_T> 36 GeV
dE_T/dΔΦ (arbitrary units)
10^2
10^1
0
90°
180°
Δ Φ

Fig. 8

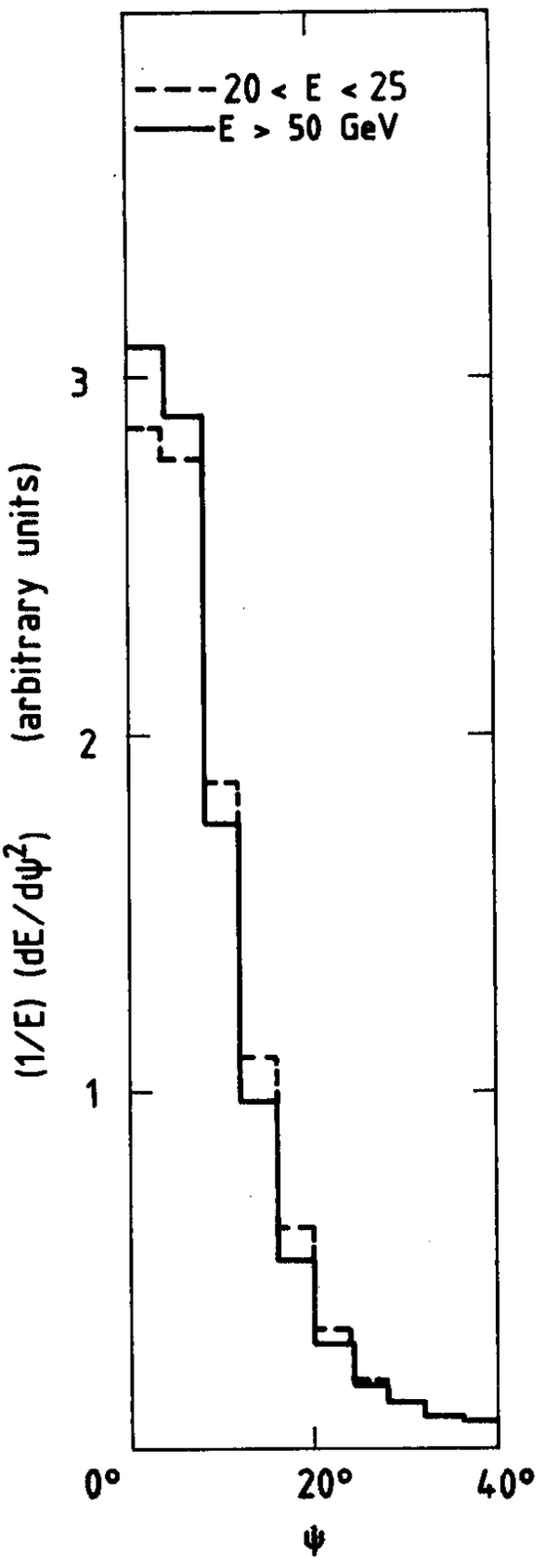

Fig. 9

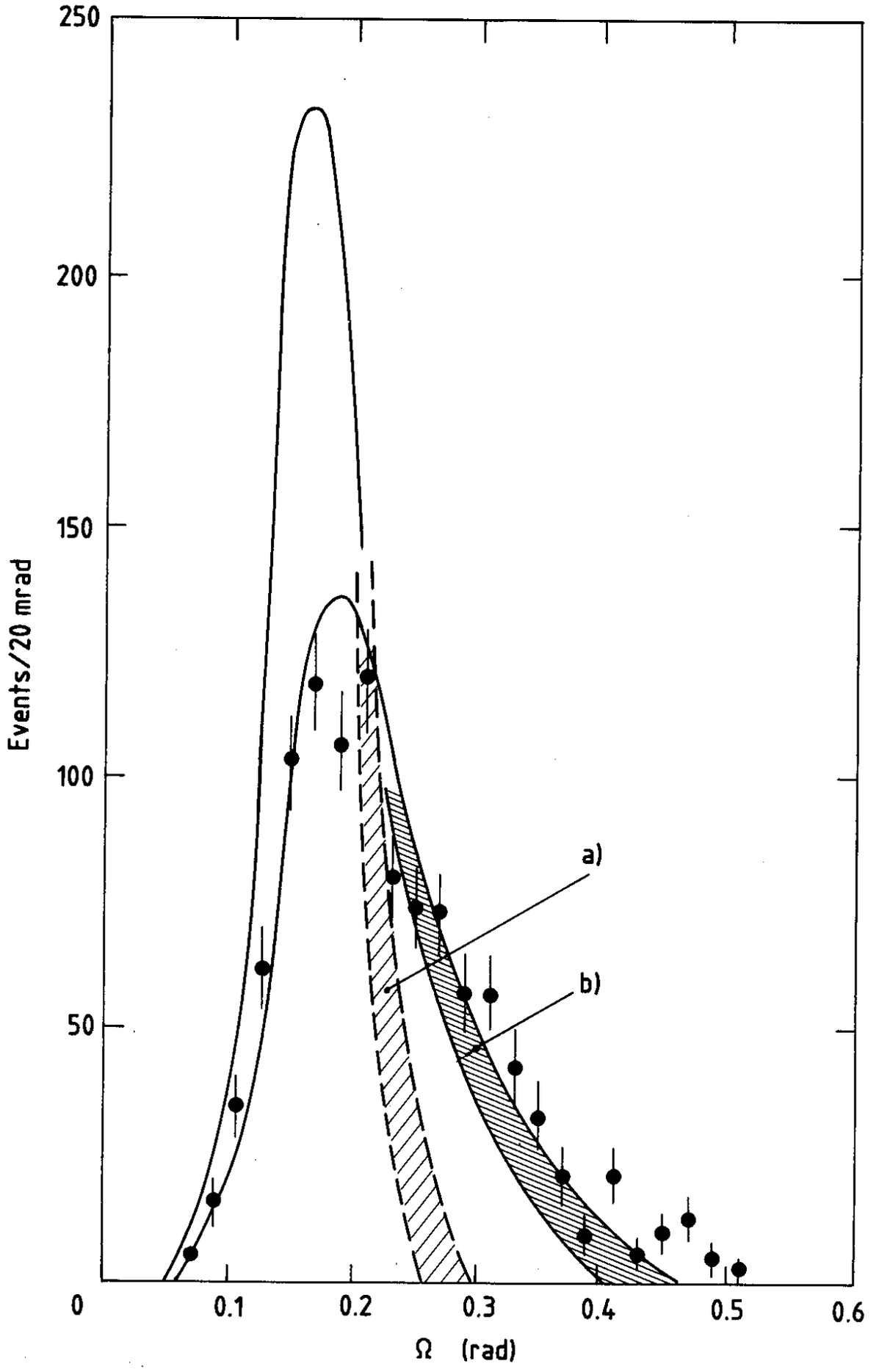

Fig. 10

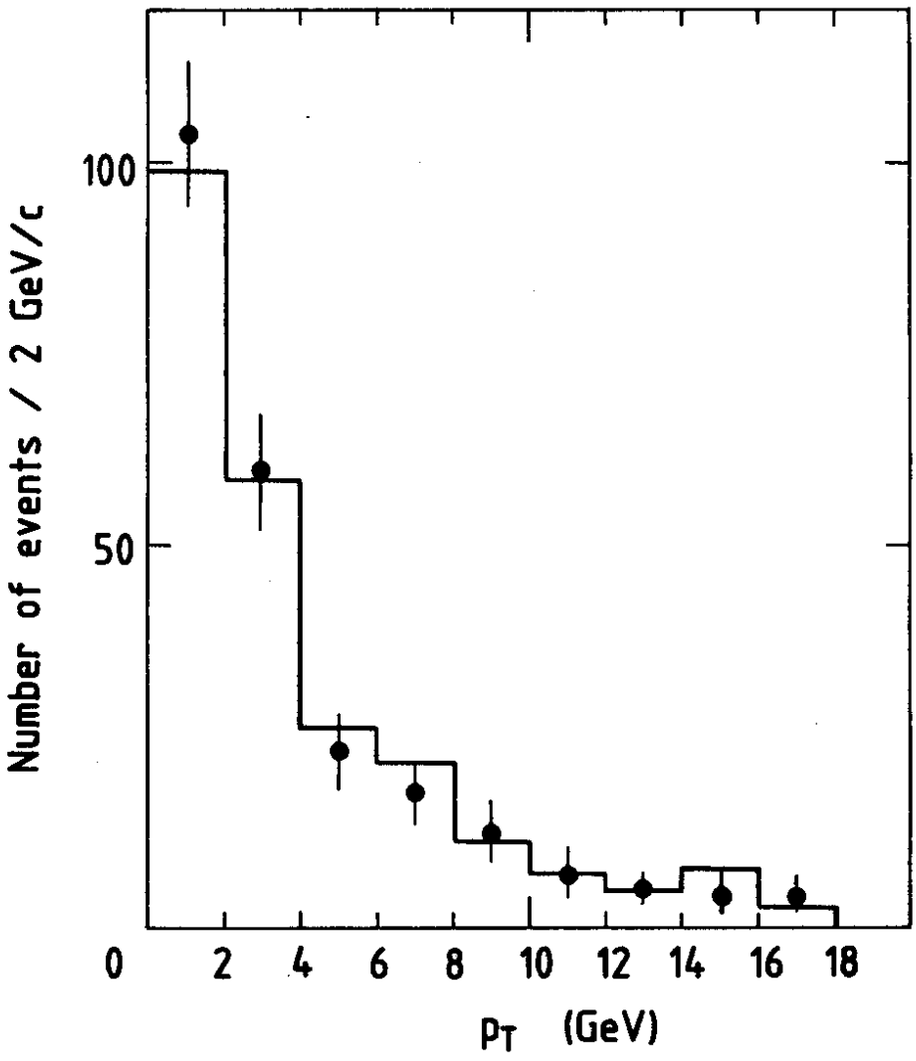

Fig. 11 a

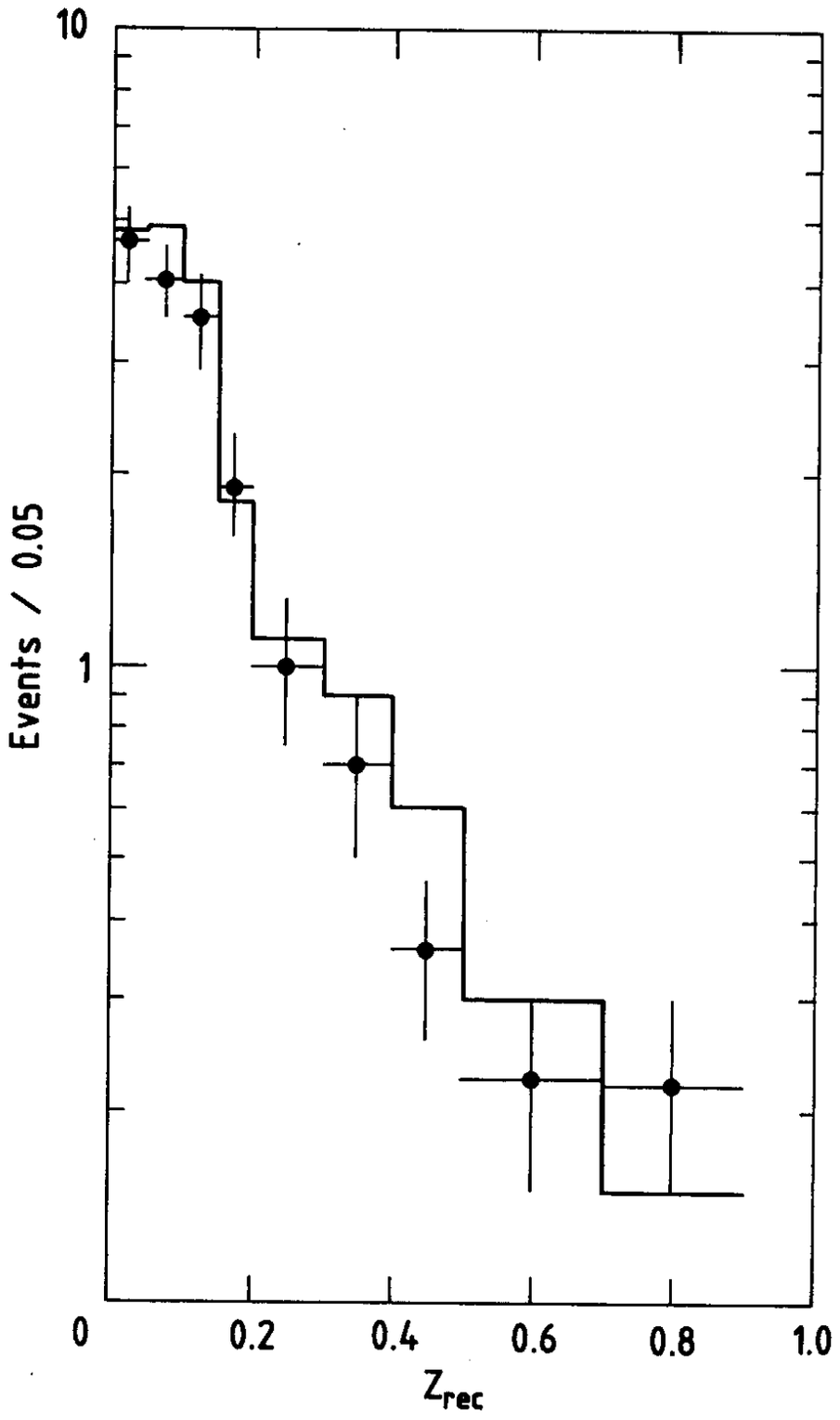

Fig. 11 b

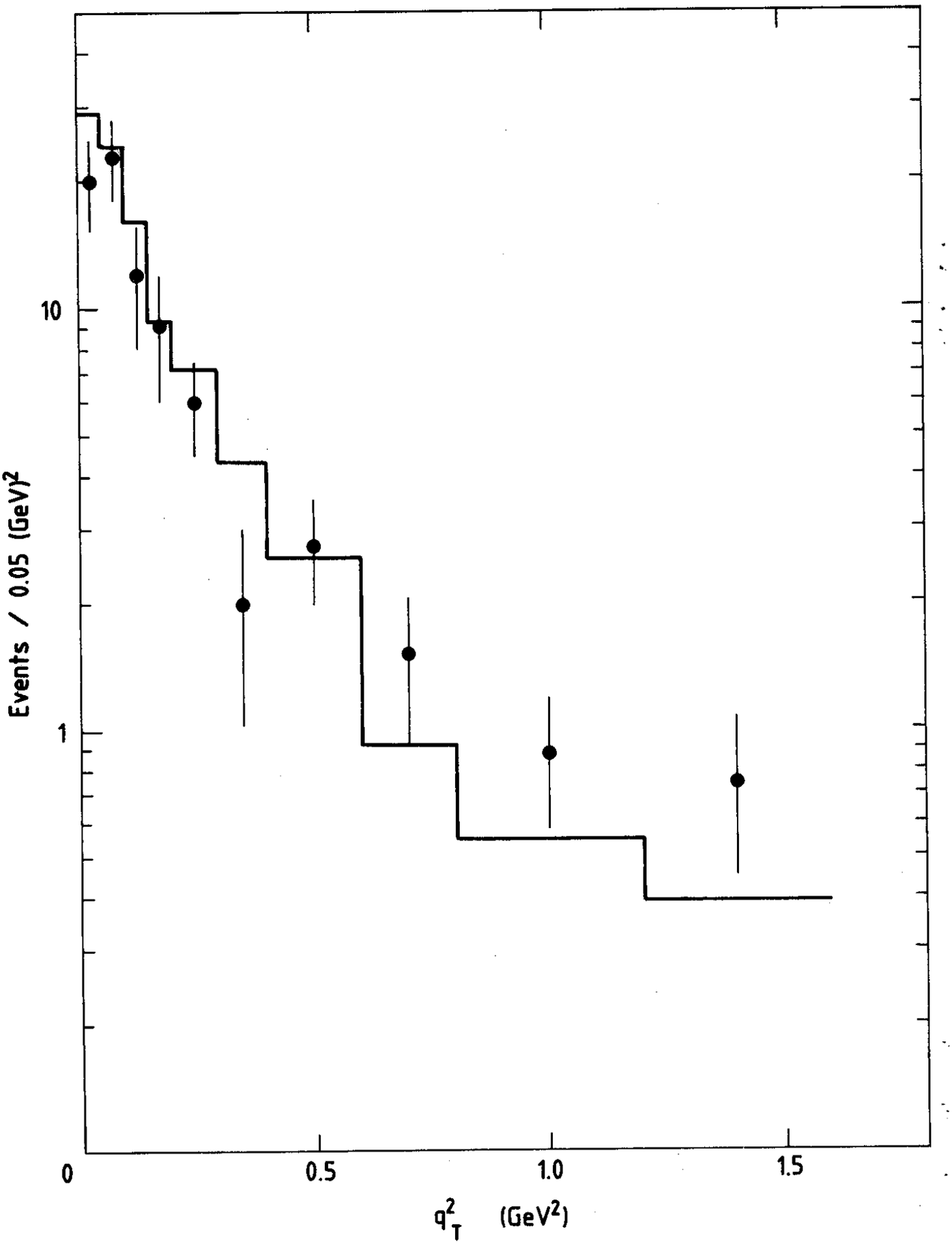

Fig. 12

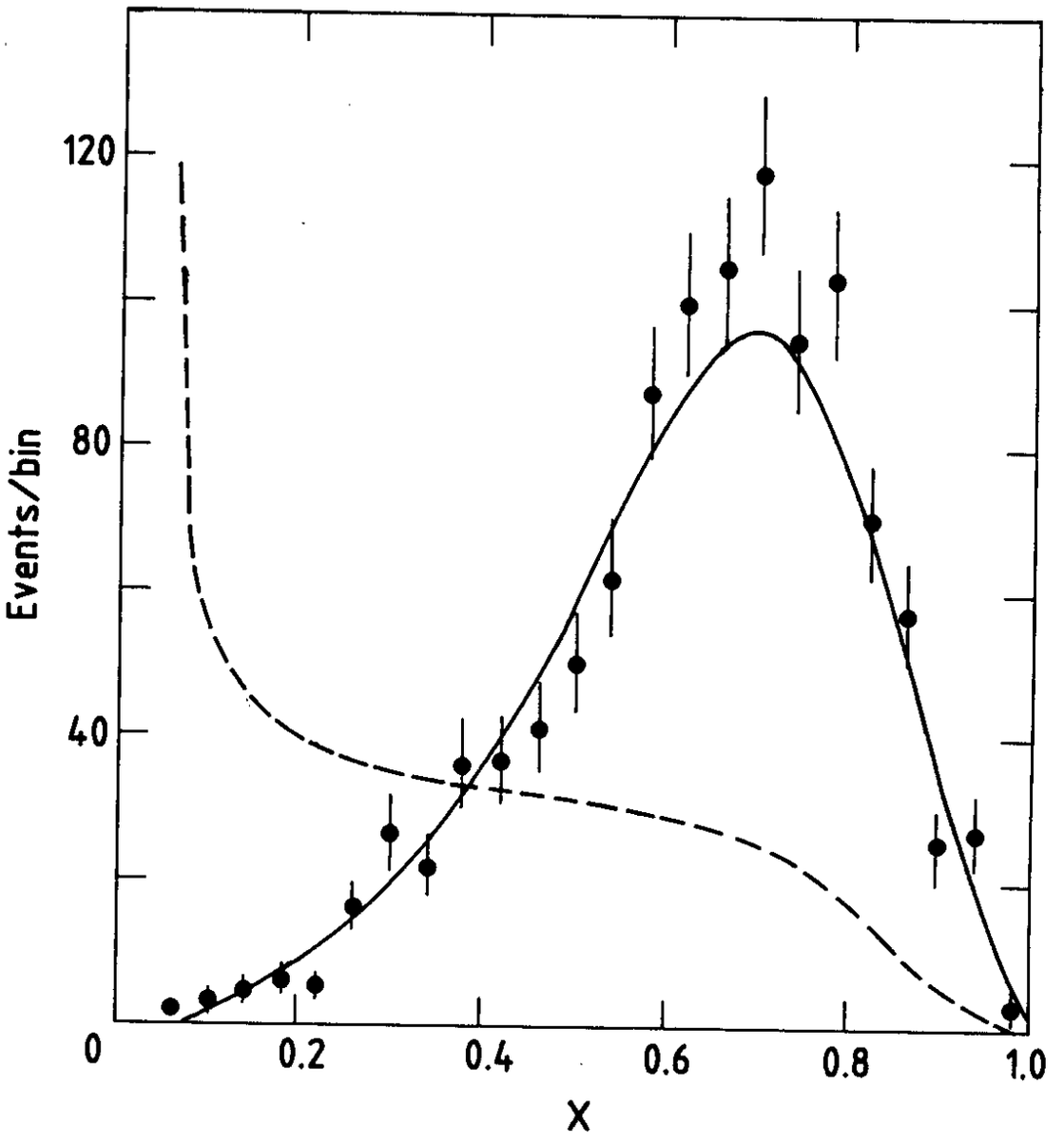

Fig. 13

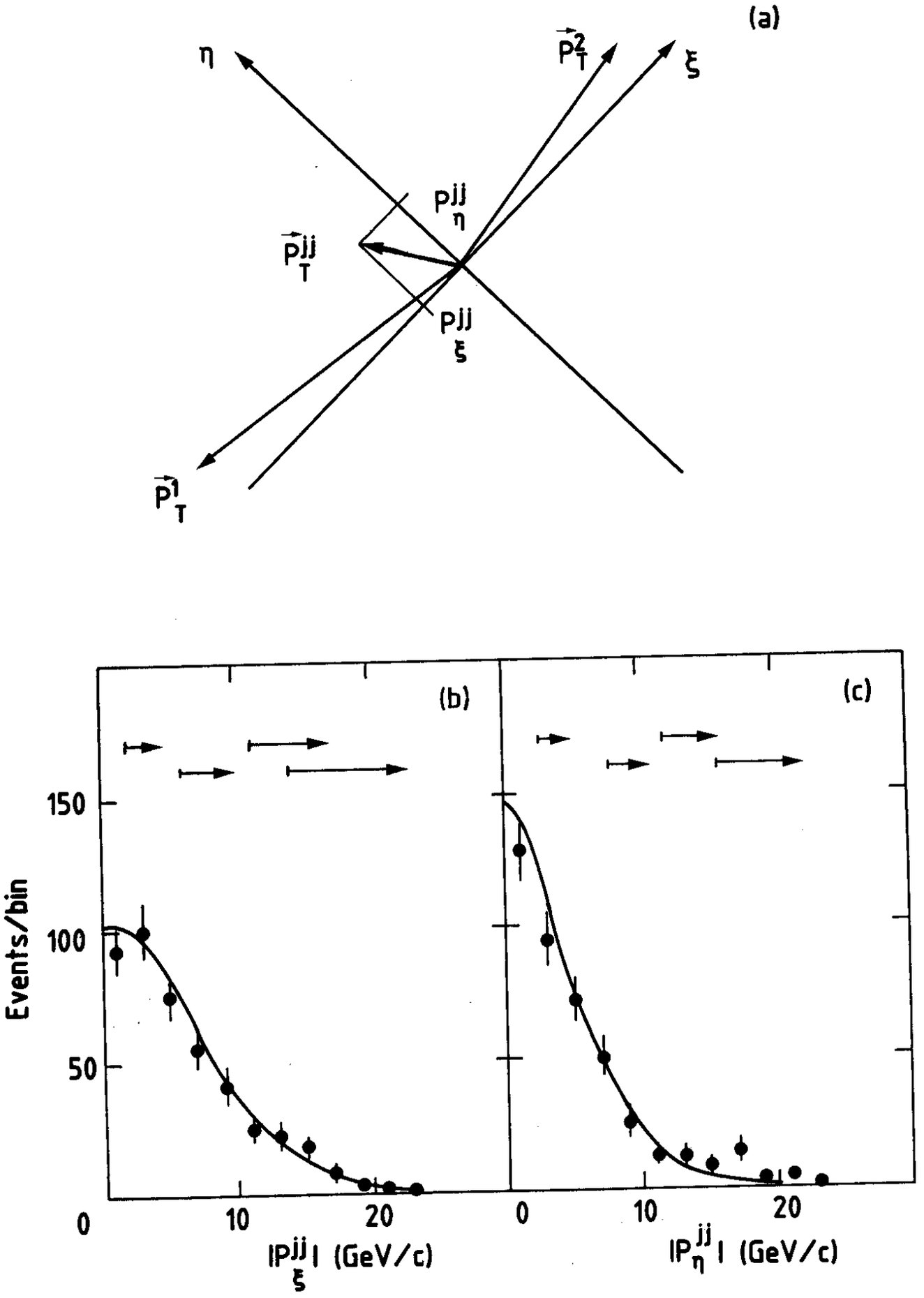
(a)
η
ξ
$\vec{P}_T^2$
P_η^{jj}
$\vec{P}_T^{jj}$
P_ξ^{jj}
$\vec{P}_T^1$
(b)
(c)
Events/bin
150
100
50
0
10
20
$|P_\xi^{jj}|$ (GeV/c)
$|P_\eta^{jj}|$ (GeV/c)

Fig. 14

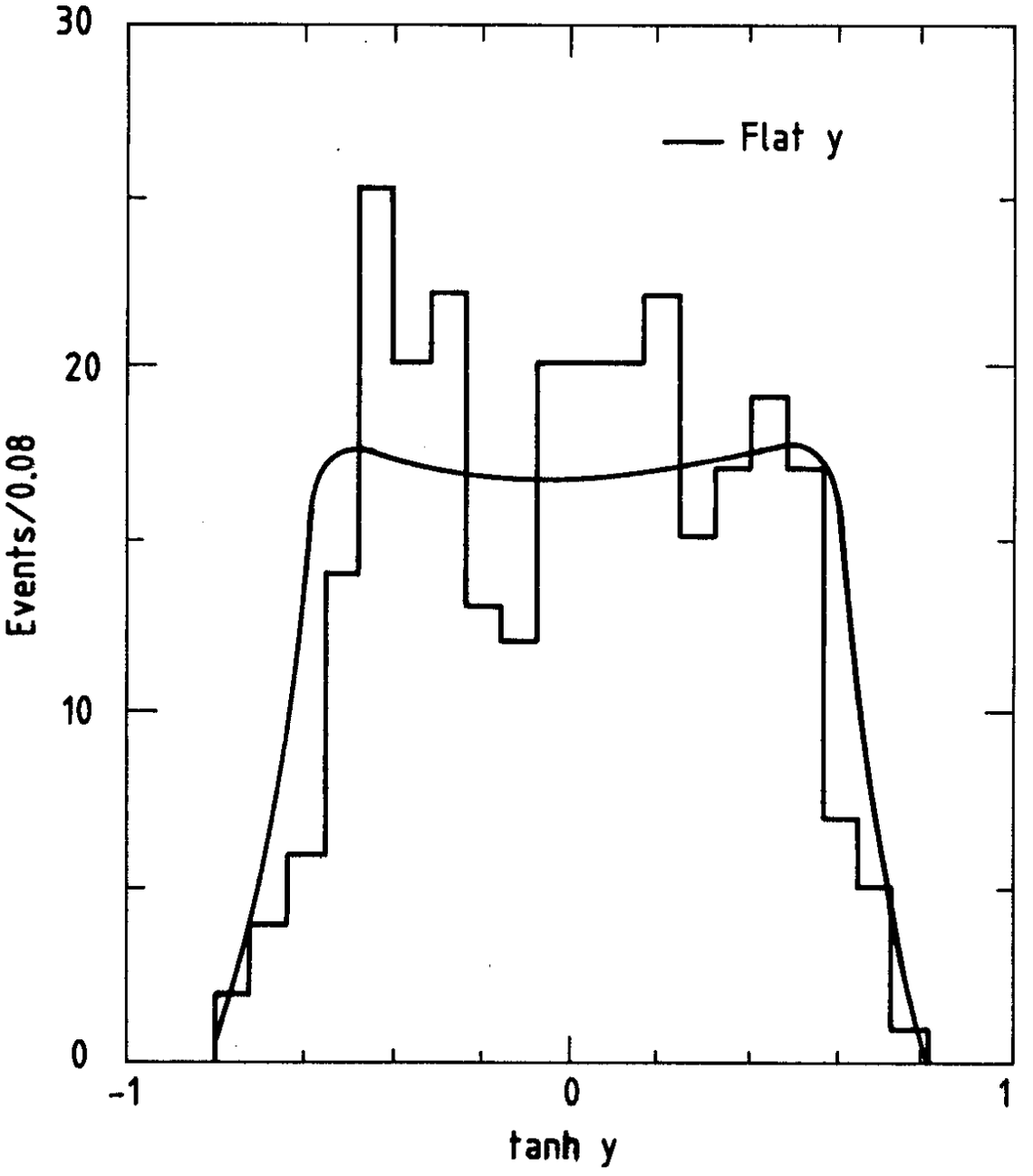

Fig. 15

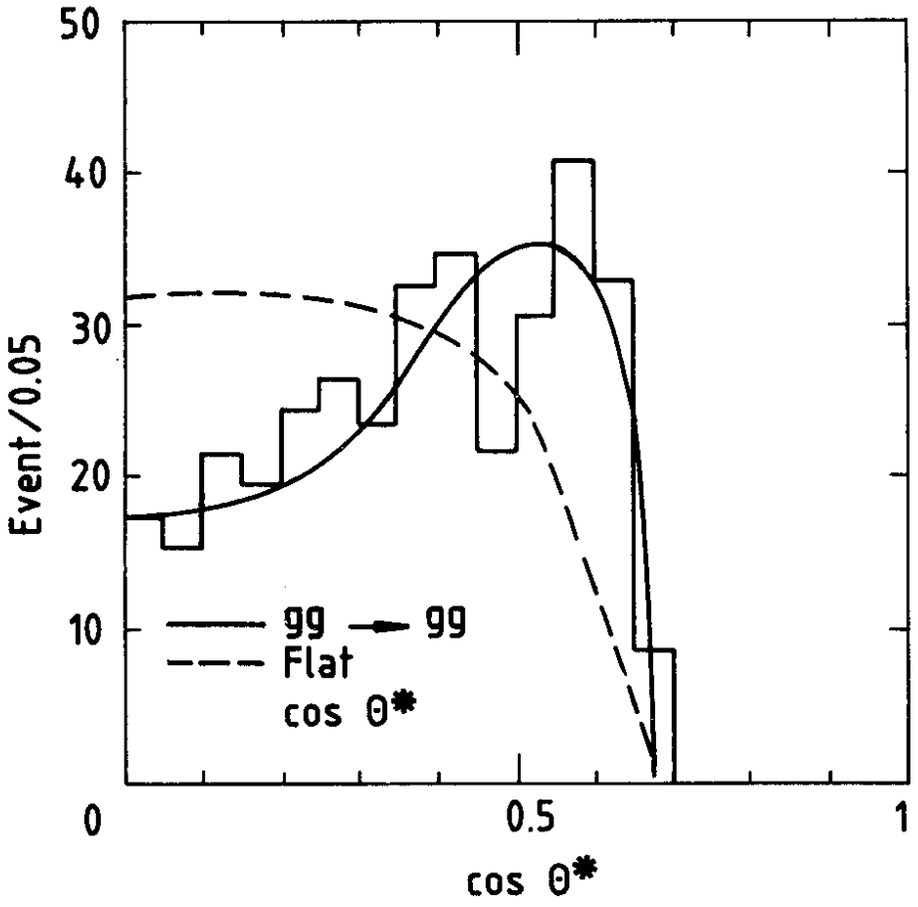

Fig. 16

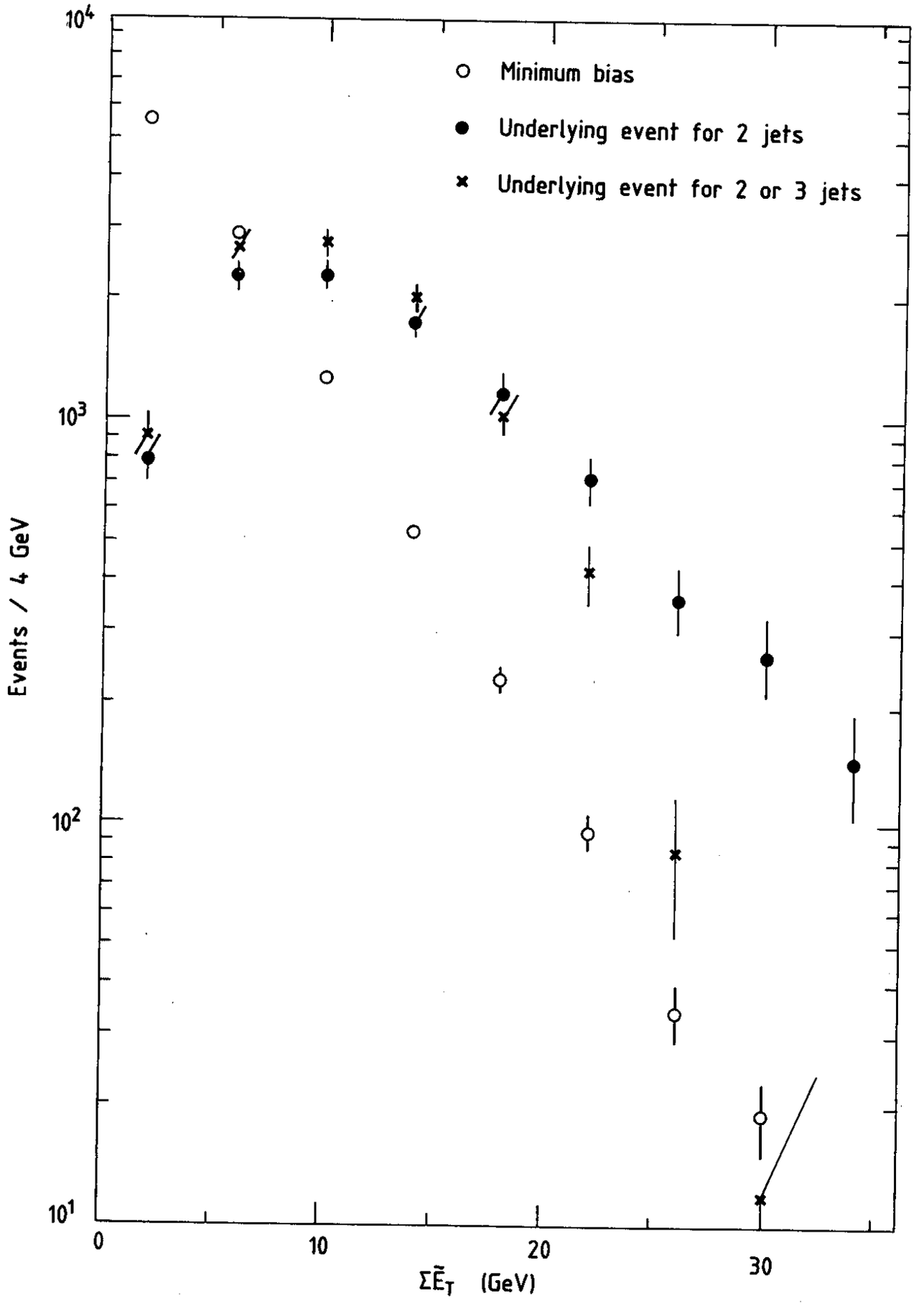
Minimum bias
Underlying event for 2 jets
Underlying event for 2 or 3 jets
Events / 4 GeV
10^4
10^3
10^2
10^1
0
10
20
30
$\Sigma \tilde{E}_T$ (GeV)

Fig. 17

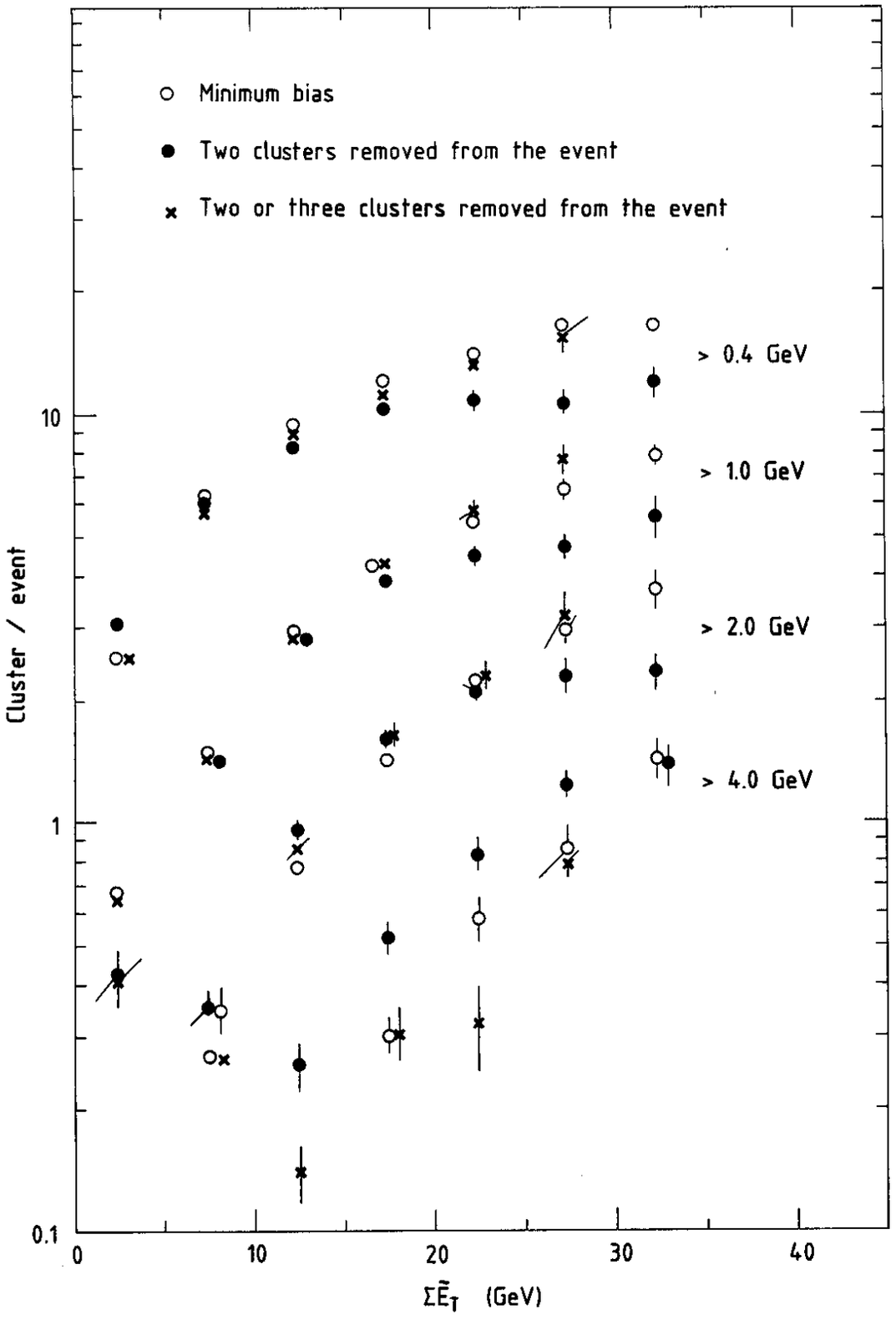
Minimum bias
Two clusters removed from the event
Two or three clusters removed from the event
> 0.4 GeV
> 1.0 GeV
> 2.0 GeV
> 4.0 GeV
Cluster / event
10
1
0.1
0
10
20
30
40
ΣẼT (GeV)

Fig. 18

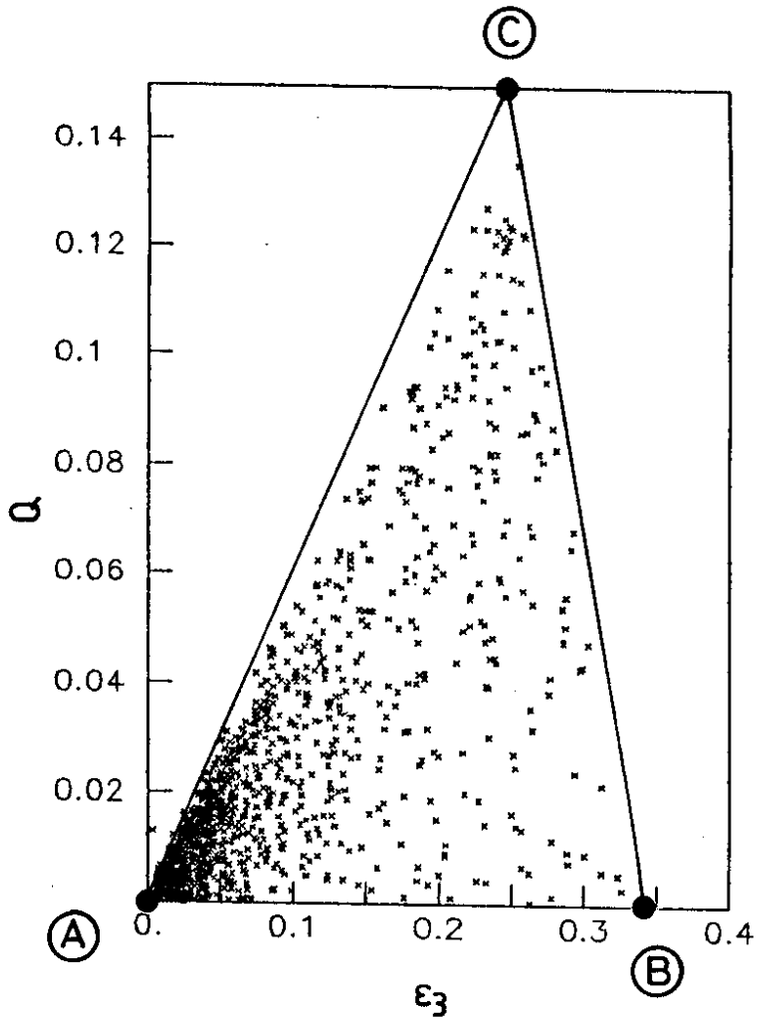
C
A
B
Q
0.14
0.12
0.1
0.08
0.06
0.04
0.02
0.
0.1
0.2
0.3
0.4
ε3

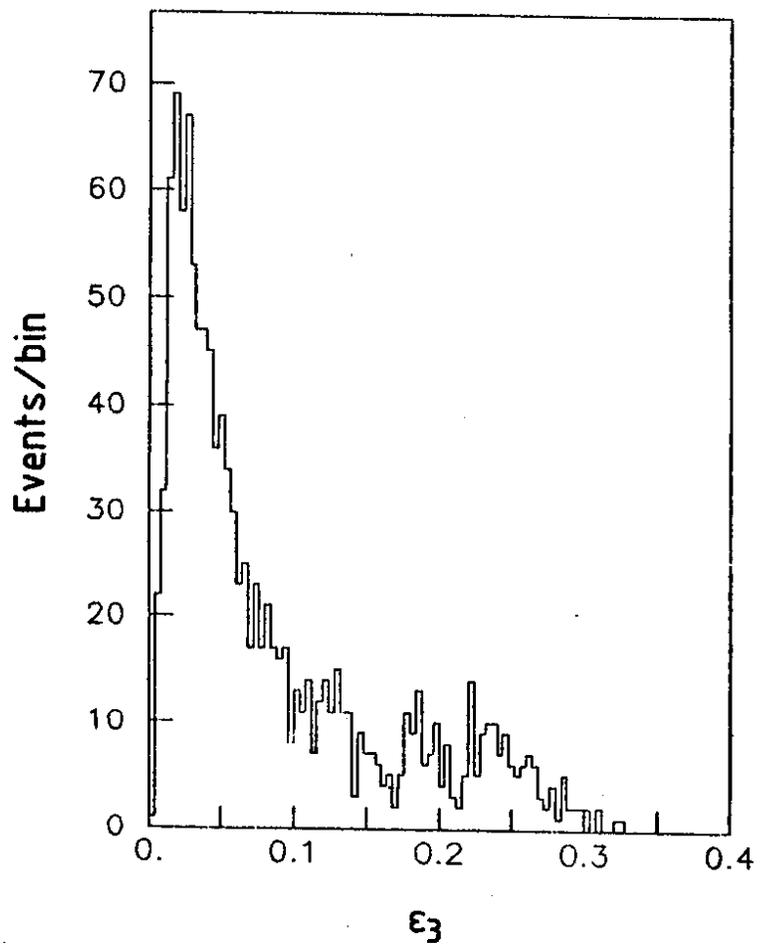
Events/bin
70
60
50
40
30
20
10
0
0.
0.1
0.2
0.3
0.4
ε3

Fig. 19

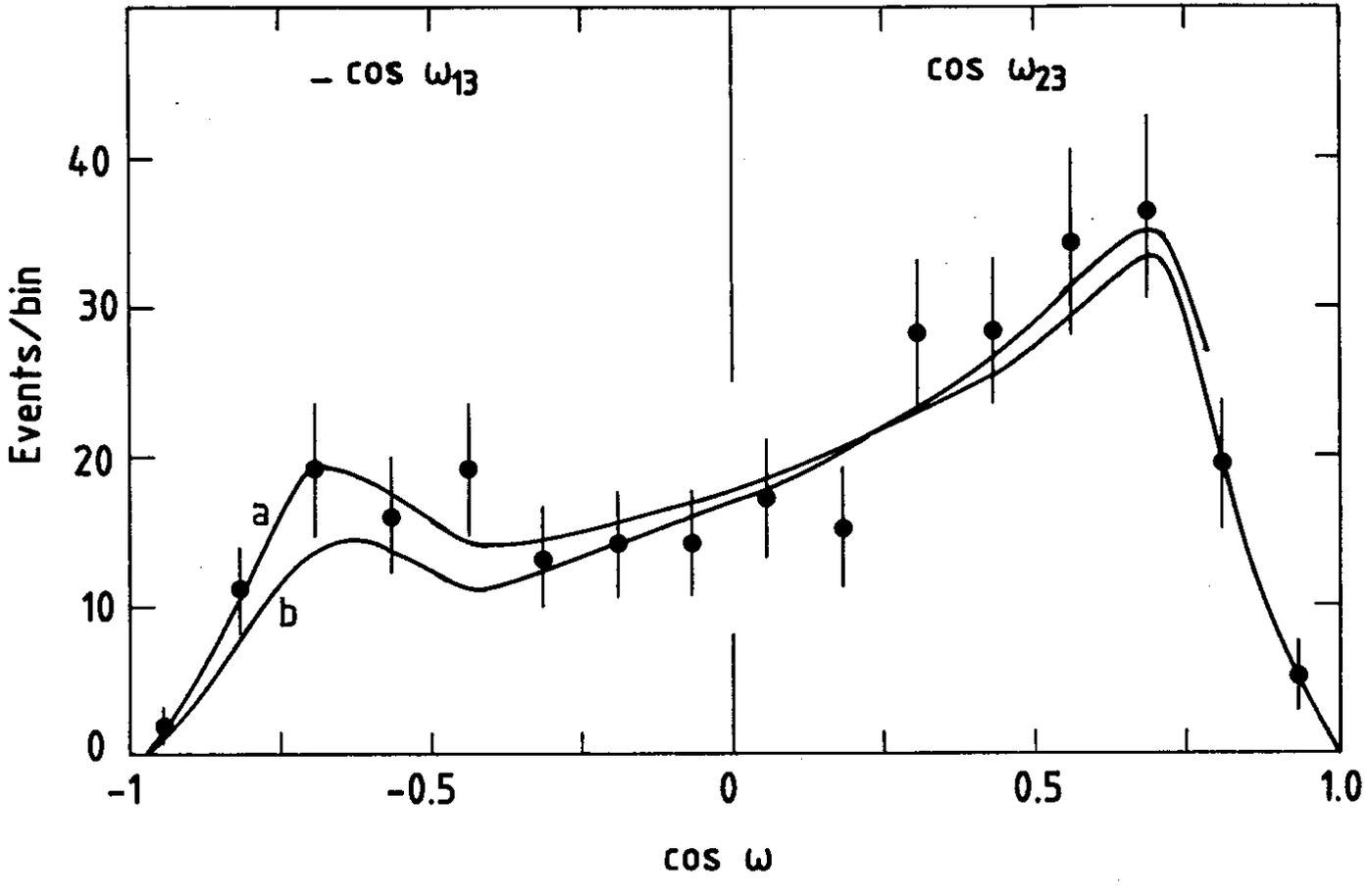

Fig. 20

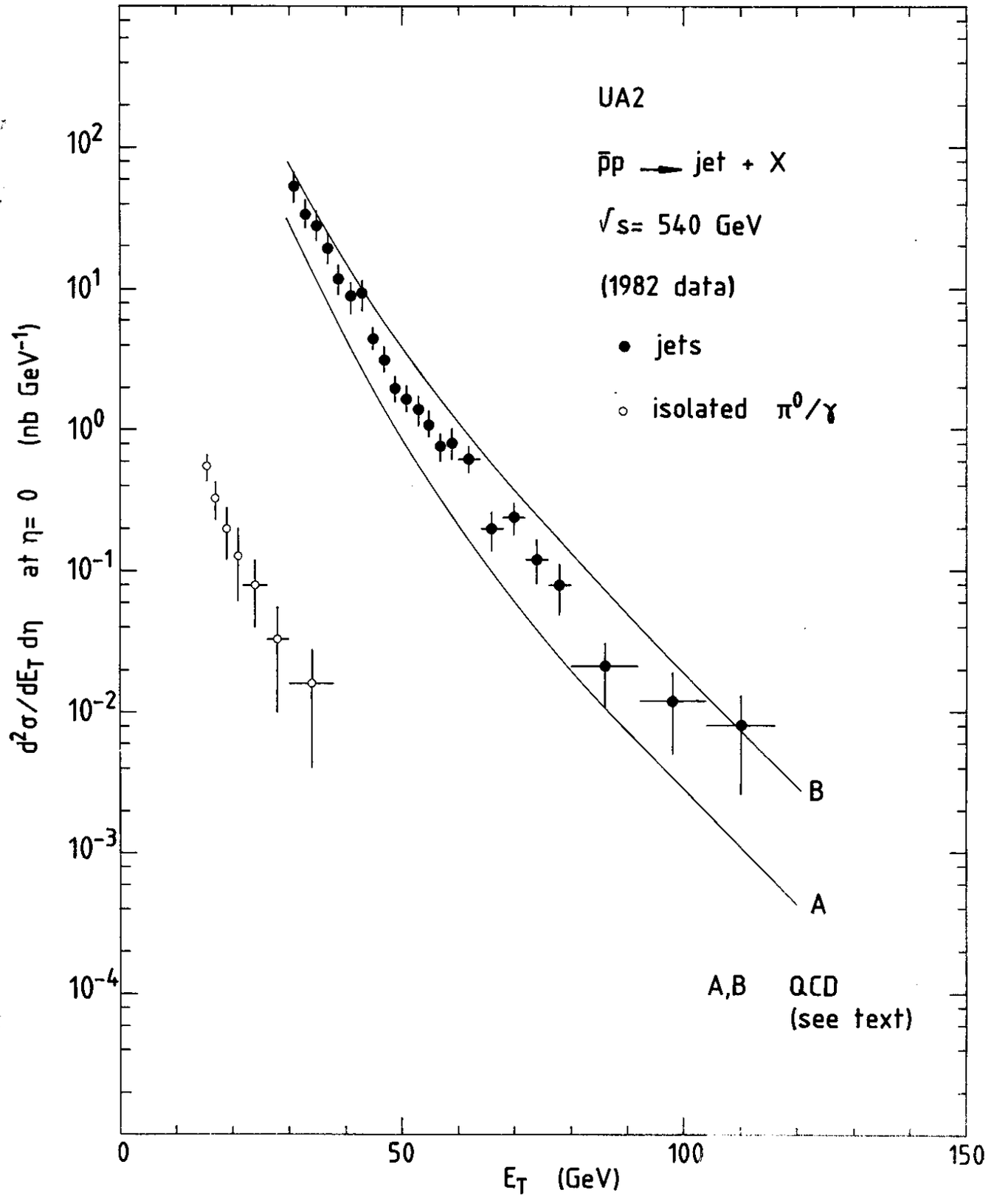
UA2
$\bar{p}p \rightarrow$ jet + X
$\sqrt{s}$= 540 GeV
(1982 data)
jets
isolated π^0/γ
B
A
A,B QCD
(see text)
$d^2\sigma/dE_T\,d\eta$ at η= 0 (nb GeV^{-1})
E_T (GeV)
10^2
10^1
10^0
10^{-1}
10^{-2}
10^{-3}
10^{-4}
0
50
100
150

Fig. 21

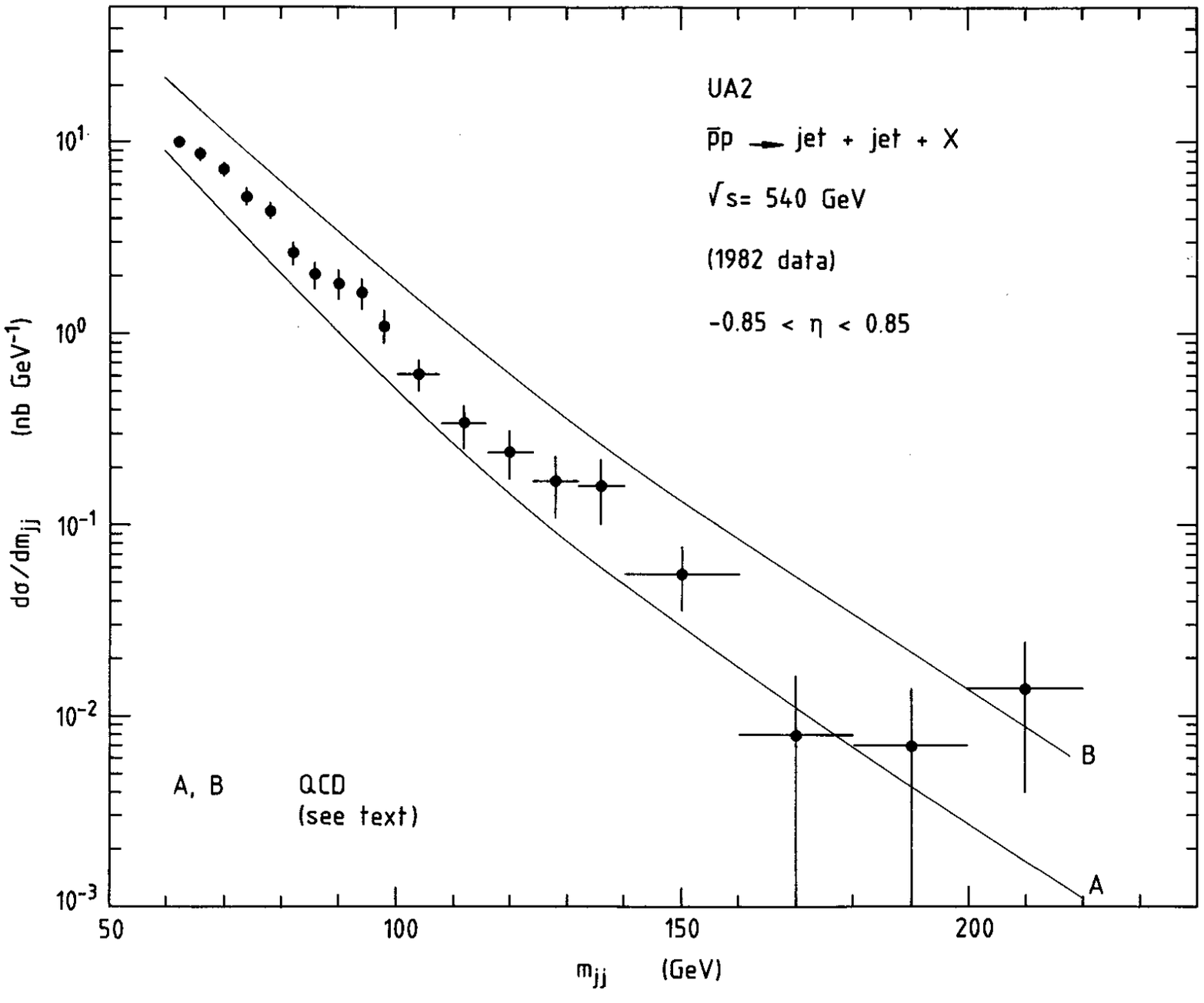
UA2
$\bar{p}p \rightarrow$ jet + jet + X
$\sqrt{s}$= 540 GeV
(1982 data)
$-0.85 < \eta < 0.85$
A, B QCD
(see text)
A
B
$d\sigma/dm_{jj}$ (nb GeV^{-1})
m_{jj} (GeV)
10^{1}
10^{0}
10^{-1}
10^{-2}
10^{-3}
50
100
150
200

Fig. 22